Separation and Purification Technology 327 (2023) 124932

Contents lists available at ScienceDirect

Separation and Purification Technology

journal homepage: www.elsevier.com/locate/seppur

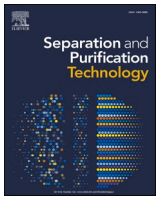

Effect of ceria particle size as intermediate layer for preparation of composite Pd-membranes by electroless pore-plating onto porous stainless-steel supports

M. Salomé Macedo [a,b], N. Acha Uriarte [c], M.A. Soria [a,b], Luis M. Madeira [a,b], J.A. Calles [c], R. Sanz [d], D. Alique [c,*]

[a] LEPABE – Laboratory for Process Engineering, Environment, Biotechnology and Energy, Faculty of Engineering, University of Porto, Rua Dr. Roberto Frias s/n, 4200-465 Porto, Portugal
[b] ALiCE - Associate Laboratory in Chemical Engineering, Faculty of Engineering, University of Porto, Rua Dr. Roberto Frias s/n, 4200-465 Porto, Portugal
[c] Department of Chemical, Energy and Mechanical Technology, Rey Juan Carlos University, c/ Tulipán s/n, 28933 Móstoles, Spain
[d] Department of Chemical and Environmental Technology, Rey Juan Carlos University, c/ Tulipán s/n, 28933 Móstoles, Spain

ARTICLE INFO

Keywords:
Membrane
Hydrogen permeation
Palladium
Electroless pore-plating
Intermediate layer
Ceria
Particle size

ABSTRACT

The use of H_2-selective membranes for ultra-pure H_2 production has been assigned as an attractive technology, particularly those based on Pd-films deposited onto porous stainless-steel (PSS) supports. The ability to incorporate thin Pd-films with enough adherence on any internal or external surfaces becomes essential to minimize their complexity and cost while improving their performance. The modification of original PSS substrates with diverse intermediate layers, especially those made of ceria, is presented as a promising alternative. In this context, the current study addresses for the first time the use of different CeO_2 particle sizes to generate an intermediate layer and facilitate the subsequent generation of a thin Pd-film by electroless pore-plating (ELP-PP). The membrane containing the smallest CeO_2 particle size (membrane S) demonstrated the lowest performance, which was assigned to the high compaction of the material and generation of cracks on its surface during calcination that consequently led to the deposition of a greater amount of Pd. On the other hand, the morphology of membranes M (medium CeO_2 particle size) and L (large CeO_2 particle size) were very similar, although the first one demonstrated a slightly smaller interparticle porosity, which led to the deposition of a more homogeneous and thinner Pd-film. Therefore, an outstanding performance in terms of H_2 permeance (5.98×10^{-4} $mol \cdot m^{-2} \cdot s^{-1} \cdot Pa^{-0.5}$ at 400 °C) was obtained for this membrane. Permeation tests with binary mixtures (H_2-N_2, H_2-CO_2, or H_2-CO) revealed a concentration-polarization effect in all cases, as well as a certain inhibition effect in the presence of CO. Finally, it should be highlighted the high stability of the membranes during the entire set of experiments, independently of the considered particle size. Thus, enough mechanical and thermal resistances can be assured for future applications.

1. Introduction

In the last years, hydrogen has been receiving widespread attention as being a clean and suitable energy vector that allows the gradual replacement of fossil fuels while facilitating the transition of the energy sector towards net zero emissions [1–3]. Nevertheless, 95 % of the profitable hydrogen produced nowadays comes from fossil fuel derivatives, particularly via steam reforming of methane (SRM) [2], leading to the formation of large amounts of carbon dioxide emissions [4]. There is however a wide diversity of other technologies that allow the production of green and/or renewable hydrogen, such as water electrolysis [5,6], thermochemical water-splitting [7,8], biomass gasification [9], and biomass derivatives steam reforming [10–12]. However, their real contribution to the hydrogen market is relatively low due to their high operating costs and low maturity level of the technologies [1].

Hydrogen has a relatively high energy density per mass unit, thus attracting great attention for many applications (*i.e.*, individual and collective transportation) and increasing its demand [13]. However, it should be noted that fuel cell vehicles (FCVs) require ultra-high purity H_2 (mole fraction $\geq$ 99.97 % and CO $<$ 30 ppm [14]) – as well as the

* Corresponding author.
E-mail address: david.alique@urjc.es (D. Alique).

https://doi.org/10.1016/j.seppur.2023.124932
Received 9 June 2023; Received in revised form 26 July 2023; Accepted 25 August 2023
Available online 28 August 2023

Notation and Glossary

List of variables

E_a	Activation energy,$J \bullet mol^{-1}$
J_{H_2}	Hydrogen permeating flux,$mol \bullet s^{-1} \bullet m^{-2}$
p_{H_2}	Partial pressure of H_2, Pa
P_{H_2}	Membrane permeability towards hydrogen,$mol \bullet s^{-1} \bullet m^{-1} \bullet Pa^{-0.5}$
$P^0_{H_2}$	Pre-exponential factor,$mol \bullet s^{-1} \bullet m^{-1} \bullet Pa^{-0.5}$
P_{N_2}	Membrane permeability towards nitrogen,$mol \bullet s^{-1} \bullet m^{-1} \bullet Pa^{-0.5}$
P'_{H_2}	Hydrogen permeance,$mol \bullet s^{-1} \bullet m^{-2} \bullet Pa^{-0.5}$
P_R	Resistance to permeation, $Pa^{0.5}$
R	Ideal gas constant,$J \bullet K^{-1} \bullet mol^{-1}$
T	Absolut temperature, K

Greek letters

α_{H_2/N_2}	H_2/N_2 ideal selectivity
ΔP	Total transmembrane pressure, bar
δ_{Pd}	Thickness of the Pd-film,μm

List of acronyms

ABS	Angular backscattered detector
EDAS	Energy dispersive analytical system
ELP	Electroless plating
ELP-PP	Electroless pore-plating
ETD	Everhart-Thornley detector
FVC	Fuel cell vehicle
GC	Gas chromatograph
MR	Membrane reactor
OMC	Ordered mesoporous ceria
PSA	Pressure swing adsorption
PSS	Porous stainless steel
PVA	Poly(vinyl alcohol)
RWGS	Reverse water-gas shift
SEM	Scanning electron microscopy
SRM	Steam reforming of methane
SS	Stainless steel
VA-DC	Vacuum-assisted dip-coating
WGS	Water-gas shift
YSZ	Yttria-stabilized zirconia

Subscripts/superscripts

perm	Permeate
ret	Retentate

majority of other H_2 applications, such as hydrogenation, water chemistry and general industrial applications ($\geq$99.95 % [15]) –, therefore being necessary the development of efficient ultra-high purity H_2 production or purification methods. The purification of hydrogen can be performed resorting to diverse technologies, such as absorption amine-based methods, pressure swing adsorption (PSA) units and membrane-based technologies [11,16]. The membrane-based technologies appear as a promising alternative due to their associated advantages, namely in terms of energy consumption, operation and maintenance costs, high adaptability, and versatility for a vast variety of production rates, simple operation, compactness, and lightweight. Moreover, it is worth mentioning the possibility of being integrated in the so-called membrane reactors (MRs), thus combining both reaction and separation processes in a single device [2,17–19].

Currently, different types of membranes are being studied to be applied in both independent hydrogen-separation units and/or MRs [2,20]. Metallic membranes based on pure palladium or Pd-based alloys have demonstrated superior performances for these applications over other alternatives due to their thermal and mechanical resistances, high H_2 permeances and selectivity towards H_2, thus allowing to have an ultra-high H_2 purity stream in the permeate side [1,21]. Nevertheless, the reproducibility of the Pd-deposition process, the high cost of Pd and the long-term stability of these Pd-based membranes are the main obstacles for their successful industrial implementation. The stability of a H_2-selective membrane can be mainly affected by poisoning provoked by some chemical compounds, such as carbon monoxide, carbon dioxide, steam, hydrocarbon molecules, and/or sulphur compounds, as well as by its mechanical resistance under extreme operating conditions [2]. Major efforts are now being made to overcome these limitations, particularly their high cost, such as the development of new membrane formulations and synthesis strategies that allow to reduce the Pd amount used while still producing highly H_2-selective supported membranes. In this sense, the use of porous supports seem to be efficient in allowing the reduction of the Pd layer thickness, while being observed an increase in the H_2 permeation [22]. The final properties of the Pd-film in terms of homogeneity, thickness, adherence, and morphology will depend on an appropriate choice of the support and deposition technique. The similarity between the thermal expansion coefficient between Pd and stainless steel (SS) ensures a good performance of those membranes. However, SS supports typically present a rough surface with large pores, turning the incorporation of ultra-thin and homogeneous H_2-selective films difficult [21]. To counter this, many authors proposed the incorporation of ceramic intermediate layers between the porous stainless steel (PSS) supports and top Pd-films. A wide variety of ceramic materials has been studied with this purpose, being possible to find multiple options in the literature, i.e., TiO_2 [23], Al_2O_3 [24], SiO_2 [25], ZrO_2 [26], yttria-stabilized zirconia (YSZ) [27], Fe_2O_3 [28], Y_2O_3 [29], or CeO_2 [21,30]. In this general context, Alique *et al.* [31] highlight the importance of selecting ceramic materials with thermal expansion coefficients in the region between those of the metal support constituents and the metallic H_2-selective layer, which will determine its adherence onto the porous support under operation, mechanical resistance to crack formation at high temperatures and chemical stability. CeO_2 has been suggested as an outstanding candidate for this purpose, particularly in the case of using a PSS support and Pd as the metal-selective layer [31]. Tong *et al.* [32] observed a very good stability of this type of membranes after a long-term experiment, while providing an H_2 permeability similar to the theoretical value of the pure Pd membrane.

Related to the palladium deposition alternatives, Sanz *et al.* [33] developed a process denoted as the Electroless Pore-Plating (ELP-PP), based on the conventional alternative but feeding the reactants from opposite sides of the porous substrate, which evidenced an excellent adherence between Pd and the PSS support under several operating conditions and long-term permeation experiments. The present study intends to delve deep into the versatility of ELP-PP H_2-selective membranes by analyzing in detail, for the first time to our knowledge, the influence of varying the particle size of the ceramic material used as intermediate layer. Three types of ceria with different particle sizes were activated and used as intermediate layer with the aim of determining their influence in the performance of the final composite membranes, namely in terms of H_2 permeability and selectivity, as well as the cyclic and long-term stability. In this context, the morphology of the herein prepared membranes and their respective permeation behavior with pure gases (H_2 or N_2) and binary mixtures (H_2-N_2, H_2-CO_2, or H_2-CO) have been properly assessed under two configuration modes (OUT-IN and IN-OUT) at different total transmembrane pressures (ranging from

0.25 to 3 bar) and operating temperatures (350, 400 and 450 °C). The effect of an initial thermal treatment in oxidizing conditions was also considered to analyze its potential influence on the membrane performances. Finally, the stability of the most promising membrane was assessed under the exposure to CO, a species well known to have an inhibition effect on the membranes.

2. Experimental section

2.1. Membranes preparation

As previously introduced, three different types of composite Pd-based membranes were synthesized onto PSS supports having intermediate layers formed by different CeO_2 particle sizes. Tubular porous 316L SS supports, provided by Mott Metallurgical Corp. (Farmington, Connecticut, USA), were used for the preparation of all membranes. The commercial PSS supports present an average porosity of around 20 % with a media grade of 0.1 Î¼m, an external diameter of 12.9 mm and a wall thickness of 1.9 mm. Before starting the synthesis procedure, the original PSS tubes were cut into shorter pieces having around 30 mm in length and both ends were carefully polished to ensure a tight fitting into both deposition/incorporation and H_2-permeation devices. Afterwards, each membrane endured the following successive steps: i) initial cleaning, ii) calcination, iii) activation of CeO_2 particles, iv) incorporation of the CeO_2 onto the support as intermediate layer, and v) Pd deposition by ELP-PP.

The initial cleaning of the PSS supports involved consecutive washing steps in 0.1 M HCl (Scharlab) for 5 min, 0.1 M NaOH (Scharlab) for 5 min and 96 % v/v ethanol (Scharlab) for 15 min. All the immersions were carried out at 60 °C in an ultrasonic bath with intermediate rinsing steps in distilled water to avoid contamination of cleaning solutions. Afterwards, the clean PSS supports were dried overnight at 110 °C and then calcined in air at 600 °C for 12 h in accordance to the procedure described elsewhere [28] to generate a first intermediate layer of mixed Fe-Cr oxides.

Then, an additional intermediate layer is incorporated by vacuum-assisted dip-coating (VA-DC) similarly to that described in the work of Martinez-Diaz *et al.* [21]. The main novelty of this work is focused on the use of three types of CeO_2 presenting different particle sizes (detailed description in Table 1). Before the incorporation of each material onto the calcined PSS supports, the raw commercial samples of CeO_2 were doped with Pd nuclei to ensure a good distribution of Pd-nuclei around the entire surface of each CeO_2 particle, even including the available surface for subsequent steps corresponding to the intra—particular porosity accordingly to the previous insights evidenced in the work published by Martinez-Diaz *et al.* [34]. This procedure ensures an homogeneous palladium deposition in the subsequent ELP-PP step just inside the new pores and surrounding areas of the intermediate barrier. For this necessary step, typically denoted as activation, CeO_2 particles were added into a solution containing the Pd-bath with a volumetric ratio of 1/18 and continuously stirred at room temperature. These particular conditions were previously optimized by studying the influence of volumetric CeO_2/Pd-solution ratios, which ranged of from 1/6 to 1/36. It was observed that a higher Pd load on doped CeO_2 was obtained by increasing the CeO_2/Pd-solution ratio, while a good Pd nuclei distribution around the CeO_2 particles was reached in all cases. These nuclei led to obtain an homogeneous Pd-film during the subsequent ELP-PP step, different from performing directly the plating step without any activation process. Nevertheless, even though the Pd doping yield increased with the CeO_2/Pd-solution ratio, a maximum was obtained for 1/18, thus being selected as the most appropriate condition. Moreover, it is important to highlight that the modification of the CeO_2 particles before their incorporation onto the PSS support avoids performing any traditional activation step, while ensuring a complete coverage with Pd-nuclei around the available surface of CeO_2 particles corresponding to the intra—particular porosity of the new ceramic intermediate barrier. The Pd-bath solution consisted of a mixture of 0.1 g/L of $PdCl_2$ (anhydrous, 60 % Pd basis, Aldrich) and 1 mL/L of HCl (35 vol%, Scharlab). Then, a reductant bath was added to the suspension containing the CeO_2 – volumetric ratio of 1/30 between reductant palladium baths, respectively – to reduce the Pd ions of the activation solution into metal nuclei that are homogeneously distributed on the external surface of each ceramic particle. The reductant bath consisted of 10 mL/L of N_2H_4 (hydrazine, Scharlab) and 119.6 mL/L of NH_4OH (ammonia solution 30 wt%, Scharlab). The doping step was completed after 2 h of continuous stirring at these conditions, being afterwards the doped CeO_2 particles filtered and dried overnight at 110 °C.

Subsequently, a new suspension in distilled water was prepared containing the CeO_2 particles doped with Pd (10 wt%) and 2 wt% of poly (vinyl alcohol) (PVA, 80 % hydrolyzed, Aldrich) to improve the adherence of the ceramic particles onto the PSS support. To generate the ceramic intermediate layer, the PSS supports were sealed with silicon O-rings and connected to a vacuum line to isolate the internal side of the membrane during the VA-DC process. Then, the PSS supports were introduced in the suspension for 5 min at room temperature to allow the formation of the ceramic intermediate layer on the external surface of the supports. This step was repeated twice but applying vacuum from the internal side of the support in the second cycle as described in the work of Martinez-Diaz *et al.* [35] to ensure a good homogeneity and reproducibility of the ceramic film. At this point, a relatively homogeneous but thick intermediate layer is formed, being required to adjust their thickness by soft washing with distilled water. Finally, the modified supports were dried overnight at 110 °C and later calcined in air at 450 °C for 5 h to ensure the complete removal of PVA and thus a good mechanical stability of the intermediate layer during the membrane operation.

Once the original surface of the support has been conveniently modified, the Pd layer was incorporated by ELP-PP accordingly to the experimental procedure reported elsewhere [1,21,34,35]. Succinctly, this technique, performed at 60 °C, is characterized by the use of two solutions containing the Pd source (5.4 g/L of $PdCl_2$, 70 g/L of EDTA (Scharlab) and 390 mL/L of NH_4OH and a reducing agent (N_2H_4 0.2 M), placed on opposite sides of the modified support (i.e., Pd source on the outside and reducing agent on the inside of the support) to force the occurrence of the chemical reaction only inside the pores and around their neighborhood areas. Several cycles of variable duration (initially of 2 h and finally of 7 h) were performed till the weight gain became negligible and no visible leaks on the Pd layer were observed. This fact will reflect a complete sealing/blockage of pores of the modified support with Pd. The leak tests were done by feeding pure helium at pressures up to 3 bar and room temperature while the membrane is immersed into ethanol to observe the possible formation of bubbles on the surface of the membrane caused by the permeation of the gas through eventual open pores or defects in the Pd film. In this sense, the nonexistence of bubbles indicates a complete sealing of the Pd-film and suitability to carry out rigorous permeation experiments at higher temperatures.

In a concise way, Table 2 describes detailed information regarding the composition of solutions used in the different steps, as well as the operating conditions applied.

Table 1
Properties of the different types of CeO_2 used as intermediate layer.

Membrane	Ceramic intermediate layer		
	Material	Brand	Particle size (μm)*
S (small)	CeO_2	Alfa Aesar, 99.5 %	0.07–0.1
M (medium)	CeO_2	Alfa Aesar, 99.5 %	3.4 (max. 7.5)
L (large)	CeO_2	Quimipur, 95 %	> 10

* Data provided by the supplier.

Table 2
Operating conditions, compounds and respective compositions used in the different steps throughout the preparation of the membranes.

Step	Compounds used		Concentration	Operating conditions	Observations
i) initial cleaning of the PSS supports	1st HCl		0.1 M	Temperature: 60 °C	Cleaning was done using an ultrasonic bath
	2nd NaOH		0.1 M		
	3rd Ethanol		–		
iii) Pd-doping of CeO_2 (activation step)	Pd-bath	$PdCl_2$	0.1 g/L	Temperature: 25 °C	Volumetric ratios between:
		HCl	1 mL/L	Pressure: 1 bar	CeO_2 / Pd-bath: 1/18
	Reductant bath	N_2H_4	10 mL/L	Time: 2 h	Reductant bath / Pd-bath: 1/30
		NH_4OH	119.6 mL/L		
iv) incorporation of CeO_2 intermediate layer	CeO_2 particles doped with Pd		10 wt%	Temperature: 25 °C Pressure: 1 & 0 bar	Supports in contact with CeO_2 suspension for 5 min. Step repeated with vacuum
	PVA		2 wt%	Time: 10 min total	
	Distilled water		88 wt%		
v) Pd deposition by ELP-PP	Pd source	$PdCl_2$	5.4 g/L	Temperature: 60 °C	Additional ELP-PP cycles can be performed up to complete blockage of pores (absence of He bubbles in leak tests with ethanol at 3 bar)
		EDTA	70 g/L	Pressure: 1 bar	
		NH_4OH	390 mL/L	Time: at least 4 cycles of 2 h and 4 cycles of 7 h	
	Reducing agent	N_2H_4	0.2 M		

2.2. Membranes characterization

The synthesized membranes were characterized through different techniques in terms of morphology reached after the most relevant experimental steps described in the previous section.

Initially, the total amount of materials incorporated onto the support – i.*e.*, Fe_2O_3-Cr_2O_3 during step ii), Pd-CeO_2 during step iv), and palladium during step v) – was estimated by the weight gain resorting to a Kern & Sohn ABS-4 electronic balance (Balingen-Frommern, Germany) with an accuracy of ±0.1 mg. These values, particularly those related to the incorporation of Pd by ELP-PP, were used to determine the estimated thickness of the Pd film, presuming a homogeneous incorporation of the metal onto the external surface of modified tubular PSS supports.

In addition, the resulting surfaces were observed through scanning electron microscopy (SEM, Thermo Fisher PRISMA-E miscroscope, Waltham, MA USA – equipped with an energy dispersive analytical system (EDAS) for microprobe analysis) before and after the incorporation of Pd by ELP-PP. Additionally, the homogeneity and real Pd-thickness of the fabricated membranes was determined through cross-sectional views after cutting and polishing the membranes.

2.3. Permeation experiments

The permeation measurements of the membranes were performed in a device reported elsewhere [21]. The schematic representation of the experimental setup is depicted in Fig. 1.

Essentially, the experimental unit consisted in a stainless-steel cell in which the membrane is placed between two graphite O-rings to guarantee the proper sealing between both retentate and permeate sides. This cell was then placed inside an electric furnace to control the operating temperature by using a type-K thermocouple placed close to the external surface of the membrane, which was connected to a temperature controller (model 2216e, Eurotherm). Pure gases (hydrogen, nitrogen, carbon monoxide, and carbon dioxide) can be fed individually or mixed with other gases through diverse EL-FLOW mass-flow controllers (Bronkhorst High-Tech, model F-201CV-AGD-11-V), being possible to test the permeation of individual gases, or multicomponent mixtures. Both retentate and permeate stream flow rates can be measured through an EL-FLOW mass-flow meter (Bronkhorst High-Tech, model F-111B-AGD-11-V). The desired retentate pressure was controlled using an EL-PRESS back-pressure regulator (Bronkhorst High-Tech, model P-702CV-AGD-11-V), while the pressure on the permeate side was always maintained at atmospheric pressure without the use of any sweep gas.

Permeation experiments can also be carried out under two different operation modes by changing the permeation flux direction throughout the membrane. This can be done due to the presence of two four-way valves, in which the feed gas stream can be introduced from the outer to the inner side or from the inner to the outer side of the membrane, therefore being possible to study opposite configuration modes denoted as "OUT-IN" or "IN-OUT", respectively. In the first configuration (OUT-IN), the gas feed stream first meets the external Pd-film before the intermediate layer and PSS support. On the other hand, the opposite configuration (IN-OUT) forces the gases to pass from the inner to the shell side of the membrane, therefore meeting the PSS support and intermediate layer before the Pd-film.

Several permeation experiments were carried out at temperatures in the range of 350–450 °C and total transmembrane pressures from 0.25 to 3 bar – *i.e.*, total pressure difference between retentate and permeate sides – using a pure stream of hydrogen or nitrogen, or mixture of gases (H_2-N_2, H_2-CO_2, or H_2-CO). In this way, both H_2 permeabilities and ideal H_2/N_2 selectivity were determined for each membrane. The influence of the permeation flux direction was studied for all operating conditions and gas compositions. In addition, a thermal treatment with synthetic air was also performed at temperatures in the range of 400–450 °C to analyze the eventual improvement of the membranes' performance. Moreover, and aiming to assess the influence of CO on the performance of the membranes, successive cycles varying between a pure H_2 stream, and a H_2-CO binary mixture stream were carried out.

It should be stated that, before starting the set of permeation experiments, all membranes were left overnight under a pure H_2 stream at 400 °C and total transmembrane pressure of 1 bar for ensuring the stability of permeate fluxes.

2.4. Permeation performance indicators

The hydrogen permeation flux (J_{H_2}) through the Pd-based membranes was determined based on the Sieverts' law (Eq. (1)), being a function of specific parameters of the membrane and the permeation driving force:

$$J_{H_2} = \frac{P_{H_2}}{\delta_{Pd}}\left(p_{H_2,ret}^{0.5} - p_{H_2,perm}^{0.5}\right) = P'_{H_2}\left(p_{H_2,ret}^{0.5} - p_{H_2,perm}^{0.5}\right) \quad (1)$$

where P_{H_2} is the membrane permeability towards H_2, $\hat{I}_{Pd}$ is the thickness of the Pd-film, $p_{H_2,ret}$ and $p_{H_2,perm}$ are the partial pressures of H_2 in the retentate and permeate side, respectively, and P'_{H_2} is the H_2 permeance. Partial pressures of H_2 are raised to the power of 0.5 since it was considered that the diffusion of atomic hydrogen through the metal lattice of the membrane is the limiting step, as typically considered for other Pd-based membranes [18].

On the other hand, the H_2/N_2 ideal selectivity ($\hat{I} \pm_{H_2/N_2}$) was determined according to the following equation:

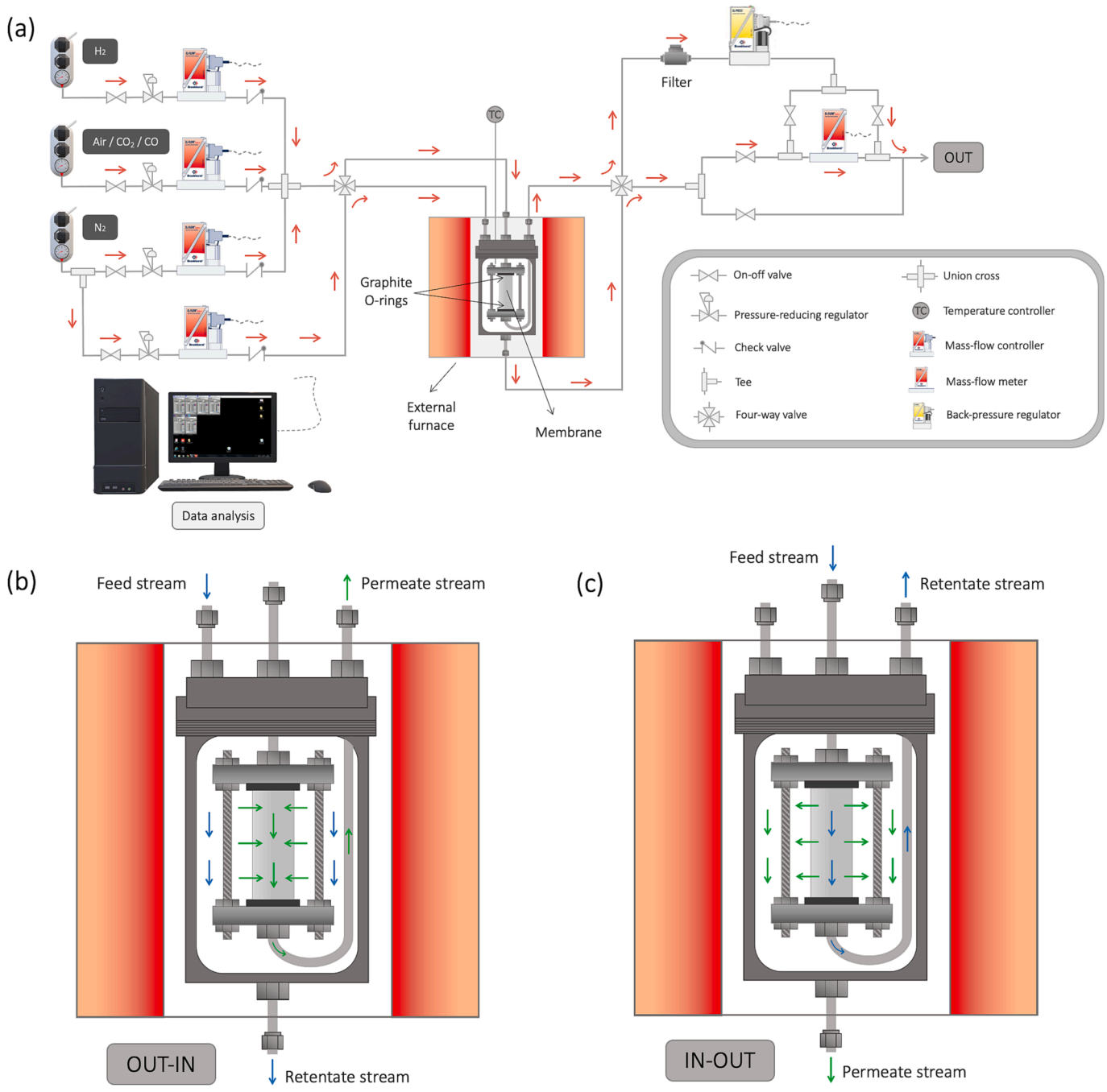

Fig. 1. Schematic representation of (a) experimental setup operating under IN-OUT configuration mode and the two operating modes of the permeation cell (b) OUT-IN and (c) IN-OUT.

$$\alpha_{H_2/N_2} = \frac{P_{H_2}}{P_{N_2}} \tag{2}$$

in which P_{N_2} is the membrane permeability towards N_2.

The H_2 permeance dependency on the temperature was assessed based on the Arrhenius-type equation:

$$P'_{H_2} = P^0_{H_2} e^{\frac{-E_a}{RT}} \tag{3}$$

where $P^0_{H_2}$ is the pre-exponential factor, E_a is the activation energy of the membrane permeation, R is the ideal gas constant and T is the absolute temperature.

3. Results and discussion

The most relevant results reached for each membrane have been divided in different sub-sections. The first one is focused on the evolution of the membrane morphology after the different steps during the synthesis procedure, namely after the incorporation of CeO_2-based intermediate layers and deposition of Pd by ELP-PP. In the following subsection, the performance of membranes during permeation is addressed. These tests were carried out at different operating conditions (temperature and pressure) by feeding pure gases (H_2 or N_2) and binary mixtures (H_2-N_2, H_2-CO_2, or H_2-CO). The long-term performance of the most promising membrane was also determined under the presence of CO to evaluate an eventual inhibition effect on the H_2 permeability. Finally,

the last sub-section compares the reached permeation results of the membranes herein presented with others found in the literature under analogous operating conditions.

3.1. Membranes morphology

The external morphology of membranes was primarily analyzed through SEM to assess the modifications in terms of both surface roughness and porosity after the incorporation of each stacked layer: Pd-CeO_2 barrier and palladium. Moreover, the real thickness of the H_2-selective Pd-film was also determined through SEM analysis of cross-sections and compared with the estimated values calculated by the weight gain during the synthesis procedure.

3.1.1. Generation of the intermediate layer

Typically, the use of PSS supports requires the modification of the original surface by the incorporation of an intermediate layer to facilitate the deposition of a thin and homogeneous Pd-film, as well as to prevent the metal interdiffusion between both layers under operation [36,37]. Fig. 2 collects the SEM images of the external surfaces after incorporating Pd-CeO_2 (particles of different sizes) to generate the ceramic intermediate layer.

Among all membranes, the one containing the smallest CeO_2 particle size (membrane S – please refer to Table 1 for the membranes nomenclature) provides a more homogeneous surface, in which the original morphology of raw support is almost lost and the new interparticle porosity cannot be distinguished. Nevertheless, some cracks appear, probably generated during the calcination of the membrane after the incorporation of the intermediate layer. This fact could be explained by the high compaction of the CeO_2 particles due to their small size and, consequently, the lack of space for thermal expansion during the calcination. This high compaction of CeO_2 particles in membrane S could also compromise the future performance of the membrane by limiting the total permeation flux or generating additional permeation resistances.

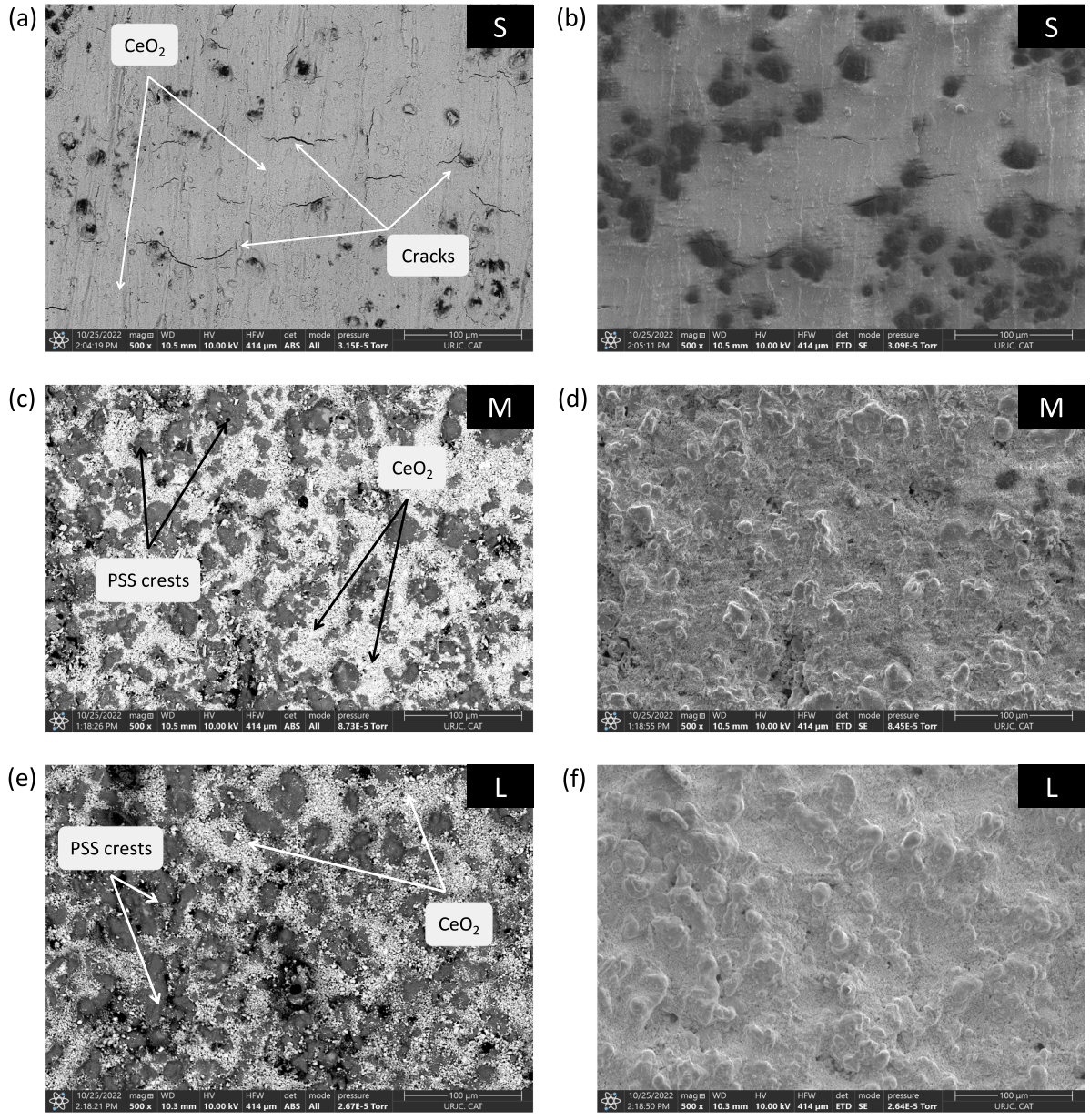

Fig. 2. SEM images of modified PSS supports after incorporation of CeO_2 intermediate layer with different particle sizes (small -S-, medium -M- and large -L-). Magnification of 500x with ABS (images from the left) and ETD (images from the right) detection modes.

Moreover, the presence of dispersed cracks on the intermediate layer will presumably require a greater amount of palladium to reach a fully dense membrane. These hypotheses will be elucidated in subsequent sections.

On the other hand, larger ceramic particles used in membranes M and L generate a noticeably different morphology, in which Pd-CeO_2 is mainly allocated in most of the original pores of the PSS support, still being possible to distinguish some remaining crests of the original support. In this manner, the ceramic particles are preferentially placed in the valleys (see Fig. 2 (c) and (e)), thus filling in the original pores of the substrate and generating a new porous structure but maintaining a certain external roughness. Despite the similar resulting morphology between membranes M and L, it seems to be appreciated a slightly greater interparticle porosity in the case of using the largest Pd-CeO_2 particles to generate the intermediate layer (membrane L) – *cf.* Fig. 2 (d) and (f) –, which will probably lead to the deposition of more Pd by ELP-P – i.e. this membrane might likely incorporate a thicker and less homogeneous Pd-film –, thus worsening its performance in terms of H_2 permeability.

Increasing the magnification up to 1000x/1500x (Figure S1 in the Supplementary Information), it is clearly observable that most of the original pores of PSS support were filled with Pd-CeO_2 in all the cases,

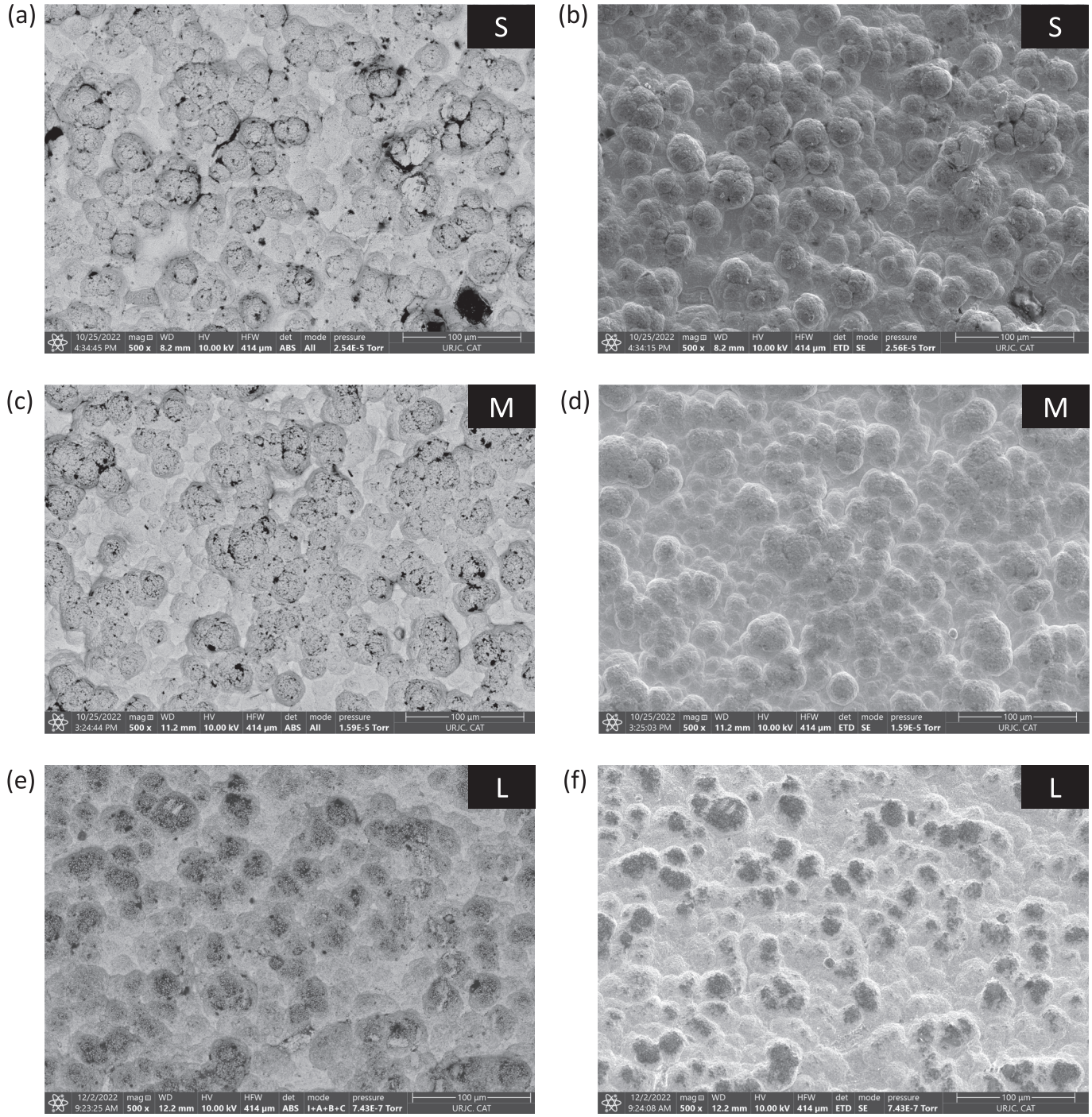

Fig. 3. SEM images of modified PSS supports after deposition of Pd by ELP-PP. Magnification of 500x with ABS (images from the left) and ETD (images from the right) detection modes.

independently of the considered particle size of CeO_2 or material used. In general, the lower the particle size of ceria, the lower the interparticle porosity and the greater the compaction of the intermediate layer. However, the use of very small particles could derive in an excessive blockage of the original substrate and formation of cracks due to thermal stress. On the contrary, large ceramic particles probably provides a high permeation capacity of the modified supports, although also generating pores that could be more difficult to be covered with Pd in subsequent fabrication steps.

In conclusion, the SEM analysis highlights the importance of using an intermediate layer for the preparation of composite Pd-based membranes onto PSS supports. Despite the presence of some pores (with small sizes in most of the cases) and cracks, these should be more easily closed by Pd in comparison to the original ones [21]. Moreover, by observing the SEM images of the different membranes, it can be suggested that the thickness of the CeO_2 intermediate layer of membrane S will be thicker in comparison to membranes M and L since the use of a smaller particle size of CeO_2 (sample S) provides a smoother surface in which the original morphology of the PSS support cannot be seen. Additionally, these results also provide a new insight about the effect of using different particle sizes of CeO_2 and, eventually, any other material used as intermediate layer for the preparation of such membranes, which clearly influences the morphology of the external surface in terms of compaction, homogeneity, and size of resulting pores, that will surely

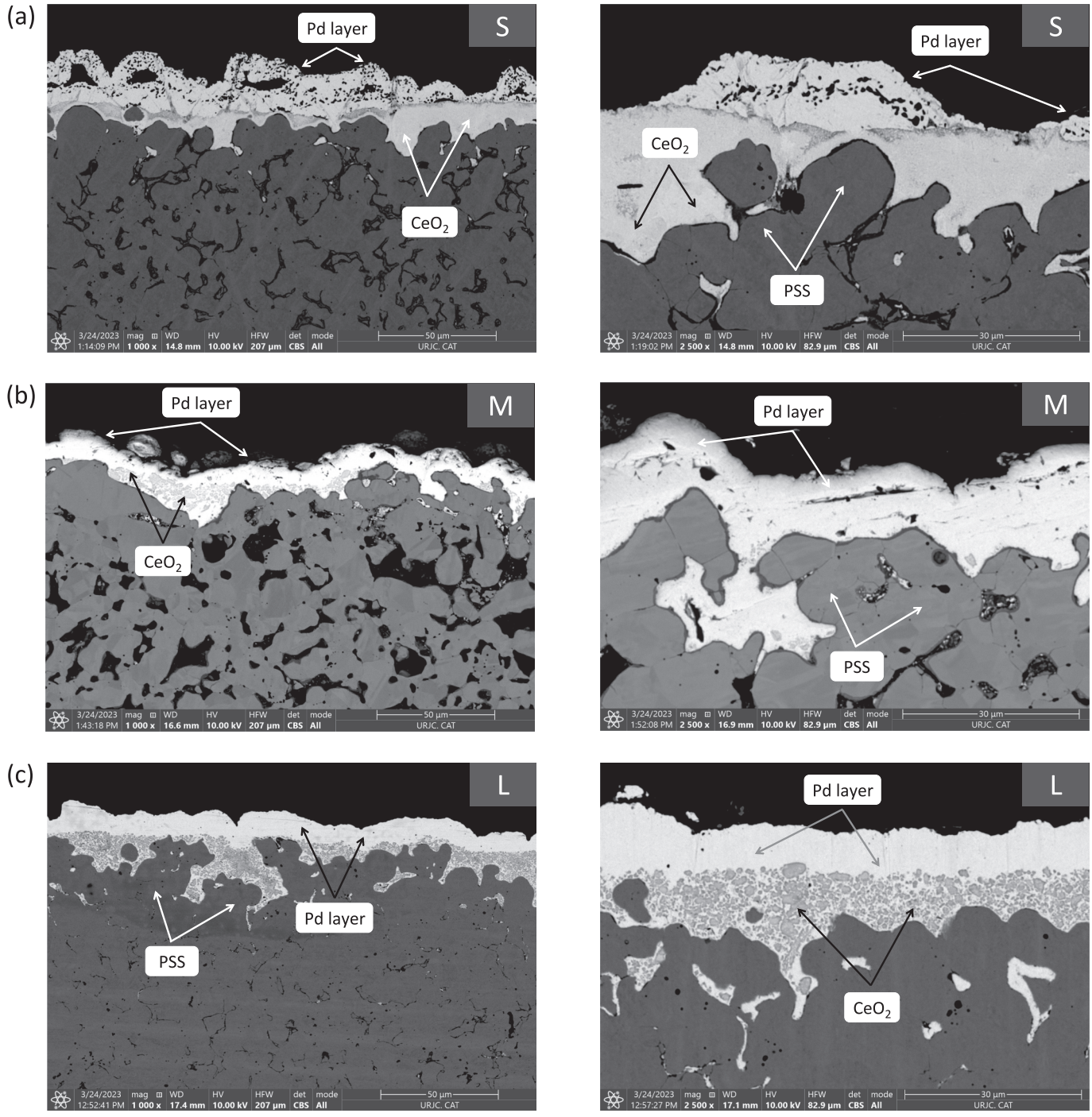

Fig. 4. SEM cross-section images of modified PSS supports after incorporation of Pd by ELP-PP of membranes (a) S, (b) M and (c) L; images obtained with a magnification of 1000x and 2500x.

affect the final Pd-thickness and overall performance of the membranes. At last, it should be emphasized that the decrease of the porous media does not hinder the passage of hydrazine through the pores during the incorporation of Pd by ELP-PP as it will be demonstrated in the next section.

3.1.2. Generation of Pd-film

The external surface of the membranes reached after the Pd-incorporation by ELP-PP is shown in Fig. 3. The SEM images reveal a very similar "cauli-flower" structure after the Pd deposition despite the use of different CeO_2 particle sizes or materials for the intermediate layer. In addition, it can be observed that an apparently homogeneous external Pd-film was formed for all membranes.

Taking a look at the SEM images of membranes obtained with higher magnification, *i.e.*, of 1000x (Figure S2 in the Supplementary Information), it can be confirmed the similarity between all the membranes, despite the marked difference reached in the morphology after the incorporation of each intermediate layer. However, some remaining pores or cavities can also be appreciated in some cases (especially in the surface taken for membrane S). At this point, it should be stated that the presence of external cavities on the Pd-film does not necessarily imply a low H_2 selectivity due to the nature of the ELP-PP method [35,38]. As a matter of fact, the Pd particles can ideally be incorporated inside the pores of the support, leading to a completely impermeable membrane towards helium, nitrogen, and other gases. Anyway, the leak test performed in ethanol at room temperature demonstrated that all the membranes become completely impermeable to helium, which evidences a complete blockage of the pores with palladium even for the membrane that contains some cavities in the external film. Additionally, in both detection modes, some dark spots are observed due to the presence of some carbonaceous species on the surface of the membranes.

3.1.3. Real thickness of the Pd-film

Regarding the final Pd-thickness reached for each membrane, besides the average estimation obtained by gravimetric analysis, cross-section views were taken (Fig. 4) to determine the real values and particular structure of stacked layers for the membranes containing ceramic intermediate layers based on different CeO_2 particle sizes.

First, it should be noted that marked differences between the diverse membranes can be easily observed. In all cases, PSS and palladium layers can be clearly distinguished in dark and light grey, respectively, although the presence of the intermediate layer made of Pd-CeO_2 (with different particle sizes) is not always evident in a similar manner. In fact, the presence of this intermediate layer can be perfectly appreciated in the case of using large particle sizes of CeO_2 (Fig. 4 (c)) as heterogeneous grains are colored as medium grey. These ceramic particles cover homogeneously the deeper areas of the PSS support, as previously discussed, while analyzing Fig. 2. Palladium occupies the space between these ceramic particles, but also generates an external film with a thickness of around 9.0 Î¼m. The infiltration of palladium between the ceramic particles (10–12 Î¼m in depth) can be justified by the nature of the ELP-PP method, in which the reduction of Pd^{2+} ions from the plating solution to metallic Pd^0 is forced to occur mainly inside the pores where the metal source meets the hydrazine solution. However, an external layer is also formed due to the high diffusion rate of hydrazine towards the Pd solution, thus being possible to reach the external surface of the modified support through the bigger pores with relative ease. On this surface, hydrazine molecules meet the Pd^{2+} ions and the formation of an external Pd-film starts. Nevertheless, due to the complete blockage of some pores before the complete formation of the external Pd-film, the morphology of the external layer has the appearance of "cauli-flower" structures with some eventual cavities, as mentioned above. Nevertheless, there is not found any interconnection between these cavities throughout the palladium thickness in the cross-section views. This particular structure, combining a top film with a certain infiltration of palladium in the new pores generated by the intermediate layer, is expected to provide a good anchoring between the stacked layers and therefore ensure enough mechanical resistance of the membranes under multiple operating conditions. Comparing the real Pd-thickness values directly measured on the SEM images with the estimated ones by gravimetric analysis (Table 3), it can be appreciated a good accordance. In fact, the average estimated Pd-thickness is maintained around 12.4 Î¼m, slightly higher than the real one determined by SEM for the top film, precisely due to the contribution of the infiltrated palladium inside the pores of the substrate.

A general similar analysis can be applied for membrane M, prepared onto a PSS support modified with medium-sized Pd-CeO_2 particles. Once again, the intermediate layer was preferentially incorporated inside all the bigger external pores of the PSS support, thus facilitating a subsequent homogeneous Pd deposition. In this case, a slightly thinner top Pd-film can be observed by cross-section images with around 6.3 Î¼m of thickness, despite estimating a contrary trend by gravimetric measurements. This can be explained by a greater infiltration of palladium into the pores. Moreover, the presence of closed and unconnected cavities in the palladium film can be also observed. This fact is even clearer in the case of using the smallest particle size for the generation of the Pd-CeO_2 intermediate layer (membrane S), where numerous cavities appear in the Pd-film. In this case, the greater compaction of the ceramic particles turns their observation more difficult in the cross-section image, although their presence in coherence with previous membranes can be related with the variation of the grey tone. Moreover, it is possible to observe that the CeO_2 intermediate layer formed on membrane S is thicker in comparison to the others due to the high compaction of the small CeO_2 particles, in which the original PSS support is practically covered by the intermediate layer. Consequently, the estimated Pd-thickness is maintained within the range obtained for the other membranes, but the marked irregularity reached on the top area can be caused by the presence of some cracks randomly distributed in the intermediate layer, as previously discussed. Moreover, a precise determination of the real Pd-thickness over the intermediate layer is very difficult.

3.2. Permeation measurements

As detailed in the experimental section 2.3, all permeation experiments with pure gases (N_2 or H_2) and binary mixtures (H_2-N_2, H_2-CO_2, or H_2-CO) were performed at temperatures and total transmembrane pressures in the range of 350–450 °C and 0.25–3 bar, respectively. Moreover, all these tests were also performed under two different configuration modes: OUT-IN (in which the gas feed stream permeates from the outer to the inner side) and IN-OUT (in which the gas feed stream permeates from the inner to the outer side). It should be emphasized that, in all experiments, the permeate was maintained at atmospheric pressure, thus avoiding the use of any sweep gas. Moreover, all the membranes exhibited a good mechanical resistance for the entire set of experiments.

3.2.1. Permeation behavior using pure gases (N_2 or H_2)

3.2.1.1. Effect of configuration mode. The permeation behavior of all membranes collected in this study was analyzed under diverse operating conditions. Firstly, tests were performed with pure gases (N_2 or H_2) to

Table 3
Estimated and real Pd thickness of membranes.

Membrane	Estimated Pd thickness (Î¼m)	Real Pd thickness (Î¼m)
S	13.4	12.5 (range of 2.9–22.1)
M	14.3	6.3 (range of 3.6–9.0)
L	12.4	9.0 (range of 6.0–12.0)

obtain the H_2 permeances (P'_{H_2}) and H_2/N_2 ideal selectivities ($\hat{I} \pm_{H_2/N_2}$) under different total transmembrane pressures and temperatures. Moreover, as previously described, the absence of defects in the membranes was assessed through a leak test with helium at room temperature, therefore indicating a good preliminary quality of membranes. In this sense, and to corroborate this fact, a set of experiments was first performed with pure N_2 at higher temperatures, in the range of 350–450 °C. As a result, no N_2 was detected in the permeate side (considering the minimum detection limit of the mass flow meter) within total transmembrane pressures of 0.25–3 bar, thus expecting a complete H_2/N_2 separation factor and a suitable mechanical integrity of the membranes. Under this premise, the permeation behavior under pure H_2 was studied at 400 °C while operating under the two different configuration modes previously described (OUT-IN *vs.* IN-OUT), as presented in Fig. 5.

In general, a good linear trend between the H_2 permeation flux (J_{H_2}) and hydrogen pressure driving force (cf. Eq. (1)) was obtained for all membranes ($R^2 \geq 0.998$), independently of the selected configuration mode. Nevertheless, it should be noted that none of these trends intercept with the origin, contrarily to what occurs for conventional Pd-based membranes that follow the Sieverts' law. This specific behavior has already been presented for other ELP-PP membranes, being attributed to the presence of an additional resistance to the permeation process (P_r) due to a certain infiltration of palladium in the porous support [1,21,34,35]. Consequently, both internal and external surfaces of the Pd film become different from each other, thus affecting the global H_2 permeating flux through the membrane. As can be seen in Fig. 6, the external Pd surface is relatively smoother in comparison to the internal one (cf. red and blue lines, respectively), which shows a great level of tortuosity provoked by the above-mentioned incorporation of Pd inside the pores of the PSS support. Therefore, the assumption of identical surfaces suggested in the Sieverts' law assumptions cannot be made and a deviation of the ideal interception of data into the origin is obtained along the x-axis for this type of membranes, meaning that there is a minimum pressure of H_2 in the retentate side to occur the H_2 permeation through the Pd layer.

The values of P_r obtained in this work at 400 °C for the different membranes are similar to others found in the literature that made use of CeO_2 as intermediate layer, belonging to the range of 11.5–24 $Pa^{0.5}$ [21,34,35] – see Table 4.

In addition, for all membranes, the H_2 permeation flux – and, consequently, the H_2 permeance – was observed to be slightly higher when operating under the IN-OUT configuration mode in comparison to the opposite one. As explained before, during the incorporation of Pd onto the porous support by ELP-PP, a certain amount of palladium is infiltrated into the pores close to the external surface. This results in a relatively smoother external surface in comparison to the internal one, which demonstrates a relatively high tortuosity (Fig. 6). Thus, the available surface area of Pd for the H_2 dissociation in the internal surface is considerably higher in comparison to the external one and therefore more H_2 can be adsorbed when operating under the IN-OUT configuration mode, leading to a higher H_2 permeance in comparison to the OUT-IN. The high mechanical stability of all membranes should be highlighted once again, particularly for the IN-OUT configuration mode in which the pressure driving forces can create a tensile stress making possible the occurrence of delamination of the Pd external layer. Since this event has not occurred for any of the membranes, it can be assumed an excellent anchoring between the Pd-film and the support.

On the other hand, it can be observed that the membrane M (intermediate particle size of CeO_2) demonstrated the highest H_2 permeance in both configuration modes, followed by the membrane L (larger particle size of CeO_2). This is line with the results obtained through SEM images, specifically those reached after the generation of the intermediate layer (section 3.1.1) and determination of the real Pd-film thickness (section 3.1.3). The SEM images of membrane M demonstrated that the Pd-CeO_2 particles were allocated in most of the pores of the support and that even the bigger pores were filled with particles, having been observed that most of the pores were nearly closed, which was definitely more convenient for the incorporation of Pd by ELP-PP through the formation of a thin (6.3 Î¼m – *cf.* Table 3 in section 3.1.3) and more homogeneous Pd-film, therefore leading to a good performance (*i.e.*, high H_2 permeation flux, and consequently high H_2 permeance, and low permeation resistance). On the other hand, the pores generated in the surface of membrane L after incorporation of Pd-CeO_2 particles were the biggest ones among all membranes, which probably turn difficult the incorporation of Pd, thus worsening the performance of this membrane due to the formation of a thicker Pd-film (9.0 Î¼m – *cf.* Table 3) in comparison to membrane M. Finally, regarding membrane S (smaller particle size of CeO_2), it was observed the formation of fissures after the deposition of Pd-CeO_2, zones in which the incorporation of Pd was probably more significant, leading to the formation of the thickest Pd-film among all fabricated membranes (12.5 Î¼m – *cf.* Table 3), thus negatively affecting the H_2 permeability of this membrane. The fact that particles were also very compacted/densified on the surface of membrane S, especially if considering the significant increase of transport resistance for reactants during the ELP-PP step throughout the smallest pores generated by this intermediate layer, might as well have contributed to its lower performance in terms of H_2 permeance and permeation resistance in comparison to the others (see Table 4). Moreover, the resulting morphology also could provide a more tortuous

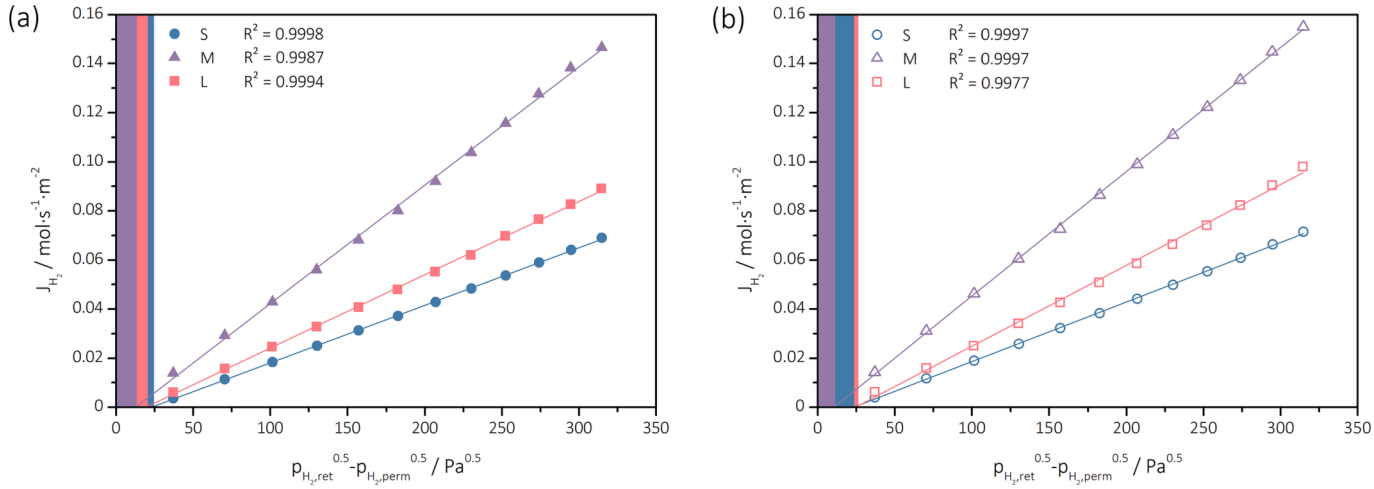

Fig. 5. Permeation behavior of the different membranes under pure H_2 at 400 °C and configuration mode of (a) OUT-IN and (b) IN-OUT.

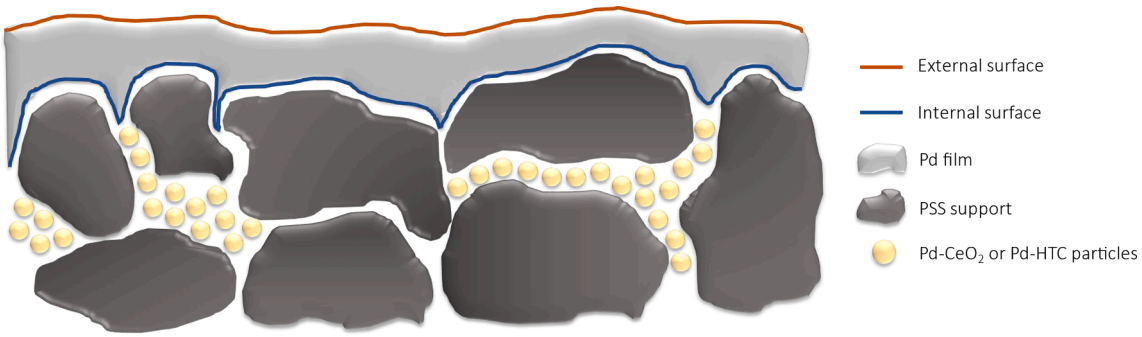

Fig. 6. Scheme of a typical Pd-based membrane prepared by ELP-PP, representing both external and internal surfaces of the Pd-film and the Pd-CeO_2 intermediate layer generated onto the PSS support.

Table 4
H_2 permeance (P'_{H_2}) and resistance to permeation (P_r) values obtained at 400 °C for the different membranes in both configuration modes.

Membrane	OUT-IN		IN-OUT	
	P'_{H_2} (mol·s^{-1}·m^{-2}·Pa$^{-0.5}$)	P_r (Pa$^{0.5}$)	P'_{H_2} (mol·s^{-1}·m^{-2}·Pa$^{-0.5}$)	P_r (Pa$^{0.5}$)
S	2.35×10^{-4}	22.9	2.43×10^{-4}	23.1
M	4.82×10^{-4}	12.5	5.07×10^{-4}	10.5
L	2.99×10^{-4}	19.2	3.30×10^{-4}	24.5

pathway for hydrogen atoms during permeation and increase the transport resistances despite reaching not so different average Pd-thickness (estimated values from gravimetric analyses) in comparison with the other membranes. In conclusion, it is clear that the use of different intermediate materials and size of CeO_2 particles, apart from affecting the reached morphology on the external surface, also affects the final thickness of the Pd-film incorporated and their tortuosity, thus affecting the membrane performance.

3.2.1.2. Effect of thermal treatment. A detailed insight regarding the effect on the membrane performance of subjecting a Pd-Ag membrane to a thermal treatment with air was firstly presented by Medjell *et al.* [39], who observed that the negative CO inhibition effect on the H_2 permeation was considerably reduced after subjecting the membrane to a thermal treatment at 300 °C in air. The positive effect of this treatment was justified by modifications in the electronic properties of the membrane surface. According to these previous results, all our membranes were submitted to an *in-situ* thermal treatment carried out at 400 °C by feeding synthetic air to both sides of the membrane. This treatment was done until no improvement on the H_2 permeation was observed. For safety reasons, all membranes were first flushed with N_2 to ensure a complete removal of H_2 before introducing to the air stream and thus avoid any explosive atmosphere. The variation in the H_2-permeance of the membranes after the treatment are collected in Fig. 7. As can be observed, a significant increase in the permeances of H_2 were reached for all the membranes and configuration modes after the thermal

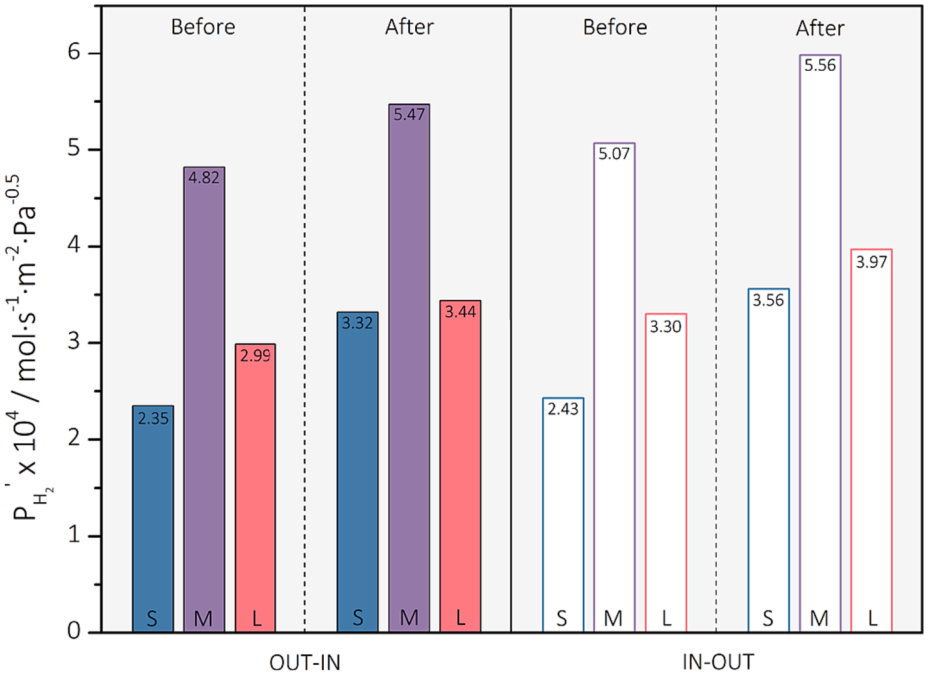

Fig. 7. Comparison of H_2 permeances obtained under pure H_2 at 400 °C in both configuration modes before and after a thermal treatment with air.

treatment. Moreover, a decrease in the permeation resistances for most of the membranes (detailed results shown in Figure S3 in Supplementary Information) was also noted. This positive effect of subjecting Pd-based membranes to thermal treatments on their permeation was also suggested by Ramachandran *et al.* [40], who described that the exposure of membranes to O_2 or air at high temperatures of 300 °C or above could have led to the formation of a thin PdO layer extending around 2 Î¼m into the surface. Nevertheless, the PdO layer should be instantaneously reduced in the presence of H_2, which was later confirmed by X-ray photoelectron spectroscopy (XPS). With this theory being refuted, it was suggested that after the thermal treatment, the number and/or type of available sites for H_2 adsorption/desorption and dissociation/

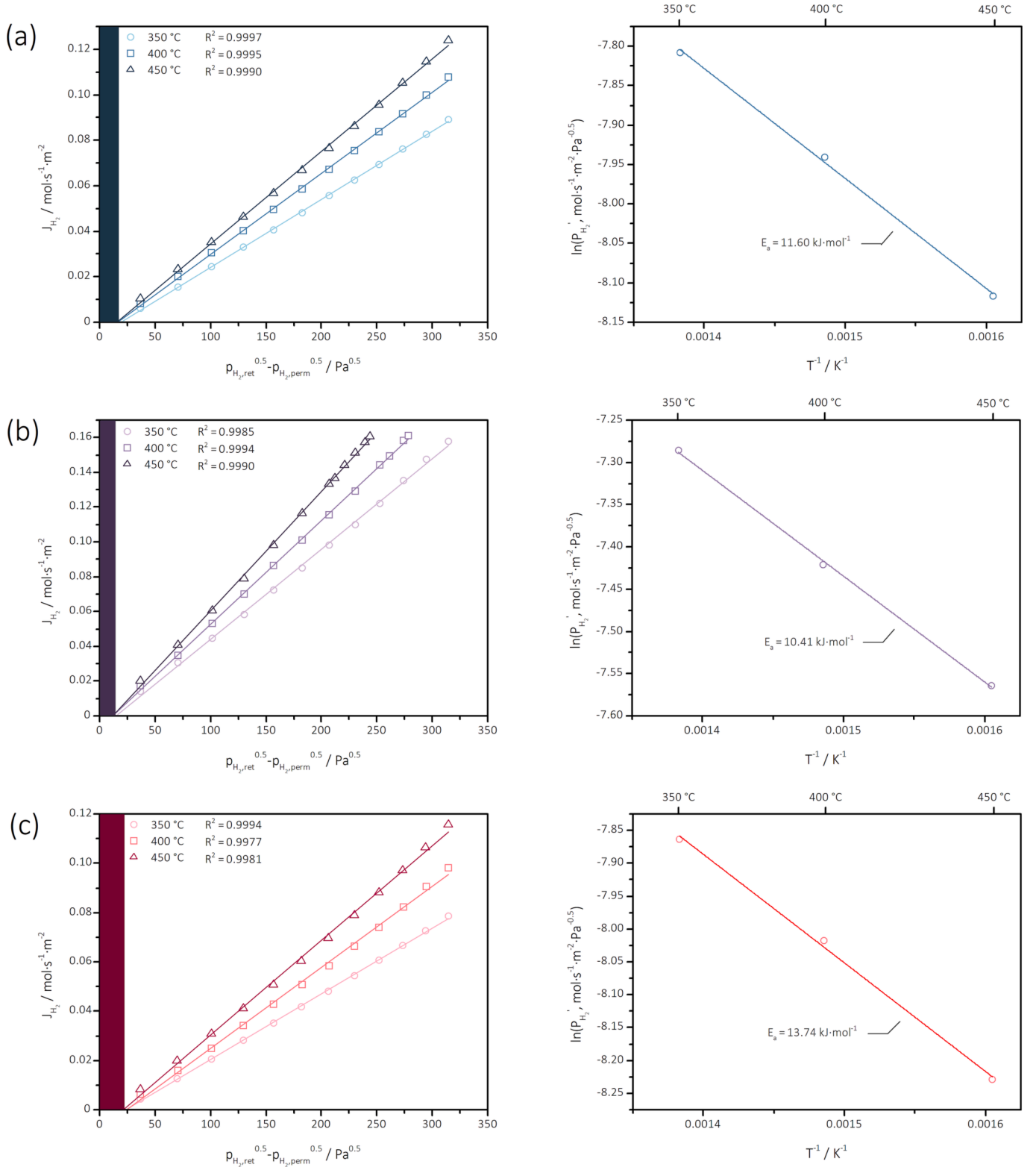

Fig. 8. Permeation behavior of the different membranes (a) S, (b) M and (c) L at different temperatures operating under pure H_2 and configuration mode IN-OUT (left side) and respective fittings to Arrhenius-type equation (right side).

recombination can be increased and/or changed, therefore enhancing the H_2 permeation rate [39]. In fact, Medjell *et al.* [39] observed a grain growth and surface roughening for membranes thermally treated with air. The grain growth was more noticed on the inner side of the membrane, which altered the grains orientation, and supposedly also the crystallographic terminations and energetics of the membrane surface. This is in line with the results obtained in this work, in which the thermal treatment provided, in general, a greater increase of the H_2 permeance under the IN-OUT configuration in comparison to the contrary operation mode (OUT-IN) with average improvements of 29 % and 25 %, respectively.

3.2.1.3. Effect of operating temperature. The influence of the operating temperature on the H_2 permeation flux under the OUT-IN configuration mode and related fittings to the Arrhenius-type equation are represented in Fig. 8 for all membranes.

The linearity of experimental data was maintained at all the evaluated temperatures in the range of 350–450 °C ($R^2 \geq 0.998$) and, as expected, higher temperatures provoke an increase of H_2 permeation through the membranes under both OUT-IN and IN-OUT configuration modes (results for the OUT-IN configuration are represented in Figure S4 in Supplementary Information). In this context, all experimental data demonstrate an Arrhenius-type dependence (Eq. (3)), being suggested that the approximation made while considering the Sieverts' law within the temperature range used is reasonably acceptable. In addition, the activation energies are very similar in both configuration modes and within the typical range demonstrated by other Pd-based membranes found in the literature (8.91–15.03 $kJ \cdot mol^{-1}$) [30,34]. Furthermore, it can also be observed that the P_r values for each membrane barely change with temperature.

3.2.2. Permeation behavior using binary gas mixtures (H_2-N_2, H_2-CO_2, or H_2-CO)

In addition to the permeation experiments with pure gases, the performance of the membrane exhibiting the highest permeation capacity (membrane M) was also assessed using binary mixtures at 400 °C and total transmembrane pressures in the range of 0.25–3 bar. For this set of experiments, H_2 was mixed with different non-permeating gases (N_2, CO_2, or CO; feed compositions of 0, 15, 30, and 45 vol%) with the aim of determining the possible appearance of resistances to mass transfer generated by the PSS support itself, any concentration-polarization effect, and/or possible inhibition provoked by certain non-permeating species.

The H_2 permeation fluxes as a function of the driving forces obtained for these experiments in both configuration modes (OUT-IN and IN-OUT) are represented in Figure S5 in Supplementary Information. As can be observed, the H_2 permeation flux trends were once again approximately linear for all binary mixtures and gas compositions in the feed, therefore allowing to assume a Sieverts'-type permeance, independently of the gas contained in the mixture and particular composition. On the other hand, despite N_2 being an inert gas that does not interact with the membranes in a significant extent, its presence clearly provokes a decrease in the H_2 permeation rate at analogous driving force. However, this decreasing trend become less relevant as the N_2 concentration in the feed increases. This specific behavior has been associated to a concentration-polarization effect on the Pd layer [41], which negatively affects the overall performance of the membranes. In this particular case, due to the impossibility of going through the Pd-film, the N_2 is accumulated onto the feed side – external or internal surface depending if it is being operated under the OUT-IN or IN-OUT configuration mode, respectively –, therefore increasing its concentration on the boundary layer close to the Pd surface due to the H_2-selective passage through the metal [30]. It is also known that the use of a porous support and intermediate layer enhances this phenomenon due to the presence of a porous structure close to the surface contributing with an additional resistance to mass transfer. This phenomenon occurs for any gas mixture, as can be observed in Figure S5, and also for mixtures with CO_2 or CO. Nevertheless, its relevance can vary depending on the properties of the compounds present in the gas mixture.

The configuration mode also demonstrates differences on the membranes' performance using binary gas mixtures. In Fig. 9, the relative H_2 permeances (normalized by the permeance obtained by feeding pure H_2) of membrane M are represented as a function of the gas composition for the different binary mixtures in both configuration modes. The decrease on the H_2 permeance due to the use of binary mixtures is substantially lower when operating under the OUT-IN configuration mode in comparison to the contrary one, being this assigned to the position of the Pd-film, which depends on the existence of a porous structure provided by the PSS support and the Pd-CeO_2 intermediate layer.

For the IN-OUT configuration mode (Fig. 10 (a)), the gas mixture is fed to the inner side of the membrane and H_2 passes through the porous media before reaching the Pd layer (internal Pd surface), where the H_2 adsorption/dissociation/recombination/desorption occurs (so-called solution-diffusion mechanism) [18]. Nevertheless, in the case of binary mixtures, gases like N_2, CO_2 and CO cannot diffuse through the Pd layer, remaining inside the pores of the support and making the permeation of additional H_2 through the Pd-film in those zones more difficult. This phenomenon, well known as concentration-polarization effect, becomes further relevant as the content of the non-permeating species increases in the feed stream, which could be expected due to the increase in mass transfer resistances. Contrarily, when operating under the OUT-IN configuration mode (Fig. 10 (b)), the gas mixture which is fed to the shell side of the membrane reaches first the Pd-film before passing through the porous media. In this case, despite the existence of some cavities and roughness on the external Pd surface, which can still provoke a certain concentration-polarization effect, the non-permeable gases can be removed from near the Pd-film in a relatively easier way by the feed stream.

Miguel *et al.* [42] studied the effect of using different volumetric concentrations of CO_2 (5–20 vol%) or CO (1–5 vol%) on the H_2 permeation flux having been observed that both non-permeating gases significantly reduced the H_2 permeability, even at low concentrations in the case of CO. In this sense, and aiming to analyze the effect of such molecules in the H_2 permeation flux, higher volumetric concentrations of CO_2 or CO in the mixtures of H_2-CO_2 or H_2-CO, respectively, were used in comparison to the ones used in the work of Miguel *et al.* [42]. As can be observed in Fig. 9, the H_2-CO mixture is the one that demonstrates a more pronounced negative effect on the permeating flux of H_2 regardless of the configuration mode. This fact can be attributed to the well-known inhibition effect associated with this species and provoked by the adsorption of CO onto the Pd metallic surface [39,42]. On the other hand, the H_2-CO_2 mixture led to a slightly superior decrease in the permeating flux in comparison to H_2-N_2. Miguel *et al.* [42] suggested that the CO_2 molecules might also be adsorbed on the surface of the Pd-film, therefore affecting the H_2 permeating flux. Other possibility could be that palladium present on the surface of membranes can catalyze the reverse water-gas shift reaction (RWGS, $CO_2 + H_2 \rightleftharpoons CO + H_2O$) at temperatures in the range of values adopted in the permeation tests, thus leading to the formation of CO that will afterwards be adsorbed on the Pd-film. To elucidate this affirmation, different volumetric concentrations of H_2-CO_2 mixtures were fed under the OUT-IN configuration at 400 °C (transmembrane pressure of 0.25 bar) and the outlet retentate stream was analyzed using a gas chromatograph (GC, Agilent 7820A) with the aim of observing the presence of CO. As can be observed in Table S1 in Supplementary Information, even though small quantities of CO have been formed assumingly through RWGS, it might be enough to decrease the performance of membranes in terms of H_2 permeation due to the CO adsorption on the Pd surface. Thus, it can be assumed that the use of H_2-CO_2 mixtures leads to a superior decrease in the performance of membranes in comparison to H_2-N_2 mixtures because of the formation of CO through RWGS and potentially due to the adsorption of CO_2 on the

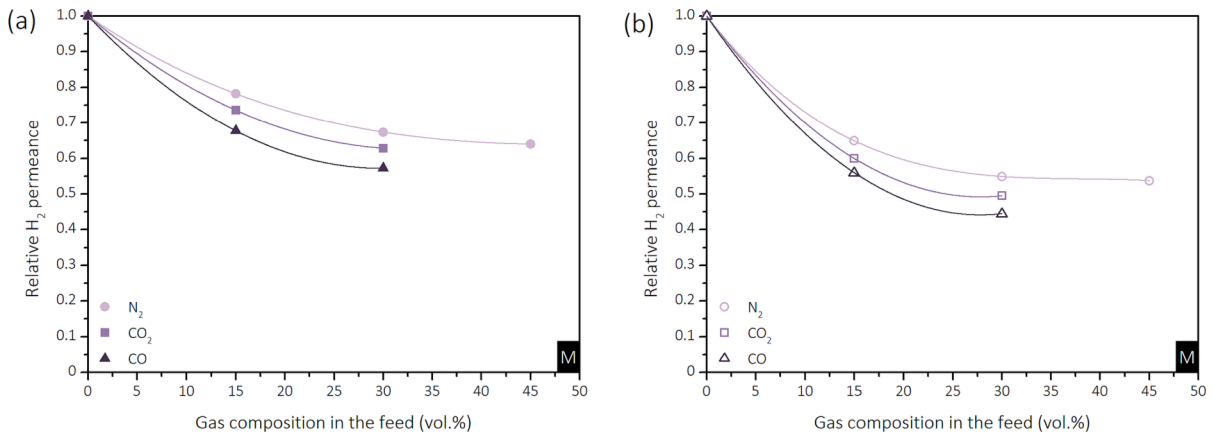

Fig. 9. Relative H_2 permeances of membrane M as a function of gas compositions of binary H_2-N_2, H_2-CO_2 or H_2-CO mixtures at 400 °C and configuration mode of (a) OUT-IN and (b) IN-OUT.

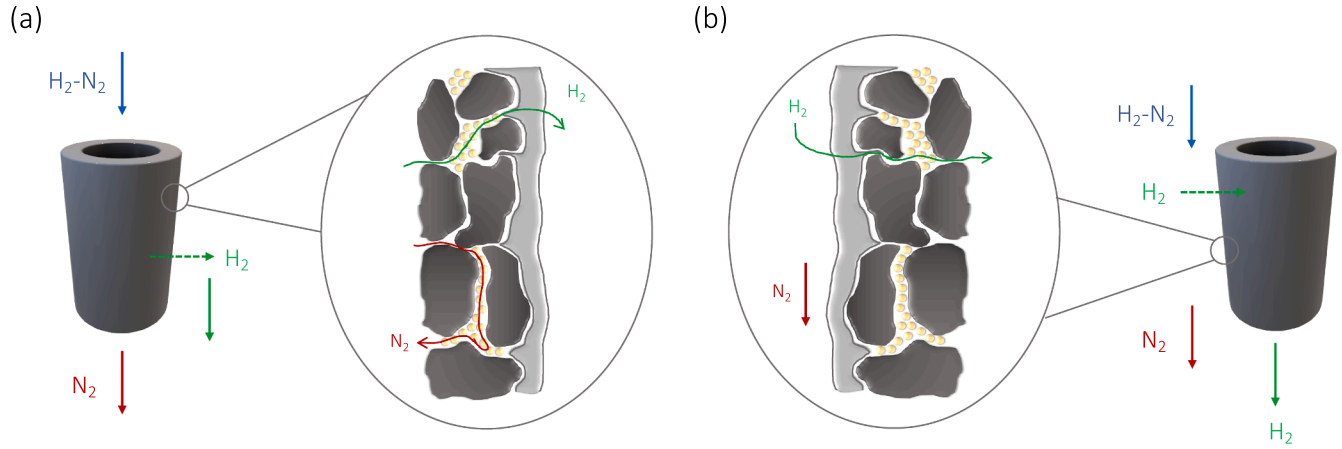

Fig. 10. Scheme of the H_2 permeation process in Pd-based membranes prepared by ELP-PP when feeding binary H_2-N_2 mixtures and operating under (a) IN-OUT and (b) OUT-IN configuration mode.

Pd surface. Nevertheless, it should be emphasized that the H_2 permeances seem to stabilize for greater dilution grades independently of the diluting gas, thus being suggested that the increase in mass transfer resistances is not linear with the content of the non-permeating gases.

These results are particularly relevant since CO_2 and/or CO are reaction products in many applications concerning H_2 production/purification, as is the case of steam reforming and water–gas shift (WGS) applications [2,10,11,43]. In this sense, as the reaction occurs, the content of non-permeating species will increase along the membrane reactor axial direction due to both H_2 permeation and CO_2/CO formation, therefore enriching the retentate stream in non-permeating species, which will consequently decrease the membrane performance, in terms of H_2 permeation, along the reactor length. This particular effect, as well as the effect of mixtures containing steam, will be addressed in future works, in which the operation considers the use of longer membranes.

3.2.3. *Stability behavior of the selected membrane*

Medjell *et al.* [39] found that CO possesses a substantial inhibition effect on the H_2 permeation flux due to its capacity to be co-adsorbed onto the Pd-film of membranes. To assess the potential inhibition effect provoked by CO, membrane M was submitted to successive cycles alternating between a pure H_2 stream and a mixture of H_2-CO (70/30 vol %) with the aim of determining the influence of CO on the performance of the membrane for longer operation times. The different feed streams were alternated every 30 min, collecting the reached results in terms of permeate fluxes in Fig. 11. As can be observed, the loss in the H_2 permeation capacity through the membrane is barely noticed along the successive cycles in the presence of CO, thus being demonstrated a good stability and the ability of the membrane to recover its original performance after multiple successive cycles under a feed stream containing CO, contrarily to what was noticed by Miguel *et al.* [42], who observed that the performance of their membrane was strongly affected by the presence of CO in a permanent manner (*i.e.*, by switching to a pure H_2 stream). Considering the results obtained by Medjell *et al.* [39] and Miguel *et al.* [42], it can be confirmed that the thermal treatment with air not only increases the performance of membranes in terms of H_2 permeance, as observed in the previous section, but it also allows to considerably reduce the CO inhibition effect on the H_2 permeation flux. This decreased negative CO inhibition effect can be produced by the induced changes in the membrane during the thermal treatment with air, which have a direct effect on preventing a permanent CO inhibition. It was suggested that the thermal treatment with air might alter the type and/or distribution of adsorption sites on the membranes surface allowing to increase the number of favorable sites for the adsorption of H_2 and to decrease the strong sites for CO adsorption [39]. So, if in the long term membranes are negatively affected by CO, a thermal air treatment with air can be done to both sides of the membrane, as suggested by Miguel *et al.* [42], allowing to fully recover the H_2 permeating flux. It appears that the reaction of O_2 with the co-adsorbed CO produces CO_2 that is purged, allowing the complete regeneration of the membrane.

Finally, it should be highlighted that all membranes maintained a very stable behavior throughout the entire set of permeation experiments, which lasted up to 5 days (120 h), despite being performed at

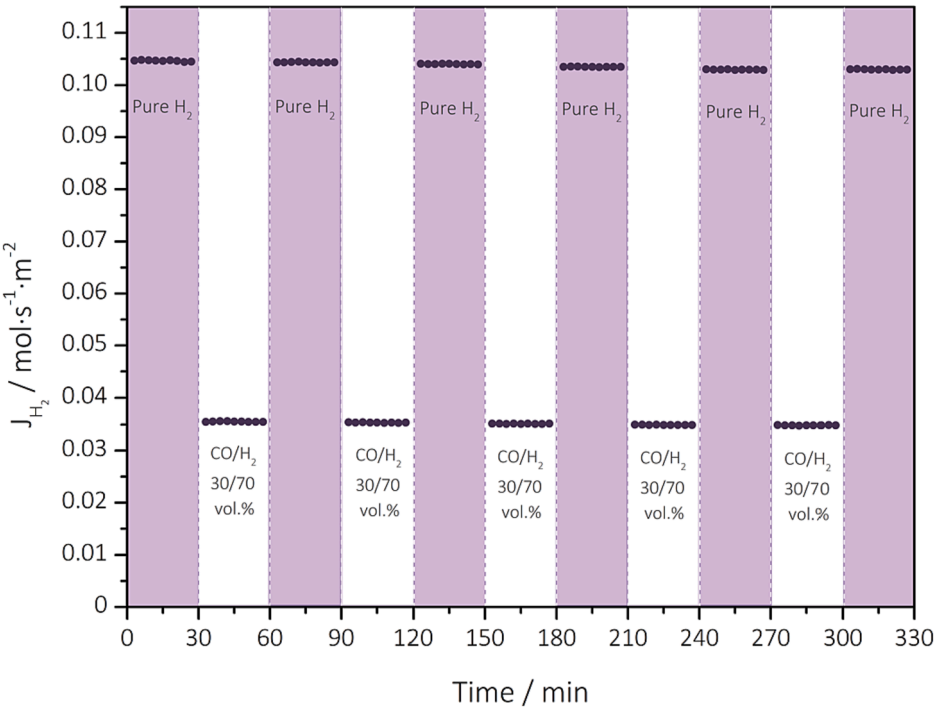

Fig. 11. Hydrogen permeating flux along time operating at 400 °C and under the configuration mode OUT-IN with different feed mixtures. The H_2 pressure driving force under the pure H_2 stream was 207 $Pa^{0.5}$, while under the H_2-CO binary mixture was 120 $Pa^{0.5}$. The membrane was thermal treated with air prior to this experiment.

high temperatures (up to 450 °C) and suffering relevant changes in pressure and feed compositions. Between each working day, the membranes were left overnight under a pure H_2 stream and none of them demonstrated any appreciable changes in the H_2 permeating flux. In addition, throughout all experiments, a good mechanical stability and integrity of membranes was observed even when operating under the IN-OUT configuration mode, which unquestionably generates tensile stress on the palladium. Still, no delamination of membranes occurred as the H_2/N_2 selectivity above 10,000 was maintained for all membranes up to total transmembrane pressures of 3 bar. Thus, it can be stated that membranes prepared by the ELP-PP method generates an excellent anchoring of the Pd layer including CeO_2 as intermediate layer, independently of the considered ceramic particle size.

3.3. Comparison with other membranes from the literature

Table 5 reports the performance under pure H_2 of some composite Pd-based membranes found in the literature. Due to the multiple possibilities for the membrane structure, the results have been delimited to those ones fabricated onto PSS supports by electroless plating (ELP) and related deposition methods. Nevertheless, it should be highlighted that the wide variety of operating conditions used in the permeation experiments, preparation method, morphological properties, structural designs, among other factors, unquestionably make a rigorous comparison between membranes difficult. For this reason, and to be possible a more restricted and focused comparison, only membranes having a Pd thickness $\leq 20\ \mu m$ were selected, with exception to the first one shown in

Table 5
Properties of different Pd-based membranes prepared onto PSS supports found in the literature.

Intermediate layer	H_2-selective film			Permeation conditions			Membrane performance		Ref.
	Composition	Preparation method	$\delta_{Pd}(\mu m)$	T (°C)	ΔP(bar)	Operating mode	H_2 permeance ($mol \cdot m^{-2} \cdot s^{-1} \cdot Pa^{-0.5}$)	α_{H_2/N_2}	
–	$Pd_{77}Ag_{23}$	–	140	400	1–6	IN-OUT	2.39×10^{-4}	∞	[44]
YSZ	$Pd_{74}Au_{26}$	ELP	5.4	500	0.6	OUT-IN	1.80×10^{-3}	4,300	[45]
Al_2O_3	Pd	ELP	7.0	320	1–4	OUT-IN	4.68×10^{-4}	92	[46]
Al_2O_3	Pd	ELP	3.8	525	4–6	OUT-IN	1.11×10^{-3}	1,800	[47]
YSZ	Pd	ELP	20	400	0–1	–	6.45×10^{-4}	340–400	[48]
TiO_2	Pd	ELP-PP	19.4	400	0.5–2.5	IN-OUT	4.59×10^{-4}	∞	[1]
CeO_2	Pd	ELP	13	500	1–2	–	3.38×10^{-5}	∞	[32]
CeO_2	Pd	ELP-PP	15.4	400	1–2	IN-OUT	5.37×10^{-4}	≥10,000	[35]
OMC	Pd	ELP-PP	10	400	1–2	IN-OUT	1.03×10^{-3}	≥24,000	[21]
Pd-TiO_2	Pd	ELP-PP	9.7	400	0.5–2.5	IN-OUT	3.55×10^{-4}	∞	[1]
Pd-SBA-15	Pd	ELP-PP	7.1	400	0.5–2.5	IN-OUT	3.81×10^{-4}	2,550	[49]
Pd-CeO_2	Pd	ELP-PP	9.1	400	1–2	OUT-IN	6.26×10^{-4}	≥10,000	[34]
Pd-CeO_2 (S)	Pd	ELP-PP	12.5	400	0.25–3	IN-OUT	3.56×10^{-4}	≥10,000	This work
Pd-CeO_2 (M)	Pd	ELP-PP	6.3	400	0.25–3	IN-OUT	5.98×10^{-4}	≥10,000	This work
Pd-CeO_2 (L)	Pd	ELP-PP	9.0	400	0.25–3	IN-OUT	3.97×10^{-4}	≥10,000	This work

the table.

In general, thinner Pd selective layers provide superior performances in terms of H_2 permeance, although some exceptions can be observed due to the specific morphology of the Pd-film (as occurs with membrane Pd-CeO_2 (M) prepared in this work). Nevertheless, most of those membranes also demonstrate limited H_2/N_2 selectivities, which is far from the intended goal, although it is not the case for all the membranes prepared in this work. In this sense, it must be remarked that membranes demonstrating high H_2 permeances are usually made of alloys containing Ag, Cu, or Au instead of pure Pd, being also typically associated with a limited H_2/N_2 selectivity, as is the case of the membranes prepared by Patki *et al.* [45], Sarić *et al.* [47] or Huang and Dittmeyer [48], therefore allowing the permeation of not only H_2 through the solution-diffusion mechanism, but also N_2 through membrane defects by Knudsen diffusion [30]. On the other hand, despite exhibiting lower H_2 permeances in comparison to the ones previously mentioned, the membranes prepared in this work showed nearly complete H_2/N_2 selectivities ($\geq$ 10,000, taking into consideration the minimum detection limit of the mass flow meter) throughout all entire set of experiments, thus being placed at the top of the list. The membrane prepared by Martinez-Diaz *et al.* [21] also demonstrated a nearly complete H_2/N_2 selectivity ($\geq$ 24,000), but providing a slightly higher H_2 permeance in comparison to the ones obtained by membrane M prepared in this work. As a conclusion, the H_2 permeances of the membranes prepared in this work range from 3.56×10^{-4} to 6.30×10^{-4} $mol \cdot m^{-2} \cdot s^{-1} \cdot Pa^{-0.5}$, values belonging to the range of those presented by other authors for pure Pd membranes, or even above, but in several cases providing considerably higher H_2/N_2 selectivities.

4. Conclusions

Three different Pd-based membranes were prepared by ELP-PP onto PSS supports being previously modified by the incorporation of CeO_2-based intermediate layer in which diverse ceramic particle sizes are considered. All CeO_2 particle sizes were doped with Pd nuclei before being incorporated as intermediate layer by VA-DC.

The morphology of membranes analyzed by SEM were clearly affected when varying different CeO_2 particle sizes in terms of homogeneity, compaction and resulting pore size of modified supports, that further affects the final Pd-thickness and conformation on the external layer of the substrates. Consequently, the overall performance of membranes was also affected. Regarding the permeation measurements performed at 400 °C, it was observed that membrane M (medium particle size of CeO_2) provided the highest H_2 permeance (5.47×10^{-4} $mol \cdot m^{-2} \cdot s^{-1} \cdot Pa^{-0.5}$), followed by membrane L (larger CeO_2 particle sizes). These results agree with those obtained by SEM, in which was observed that the Pd-CeO_2 particles of membrane M occupy most of the biggest pores of the PSS support, thus facilitating the deposition of a more homogeneous and thinner top Pd-film. The lowest performance exhibited by membrane S (smaller CeO_2 particle sizes) was linked to the formation of fissures or cracks after the final calcination treatment associated to the incorporation of the ceramic material by VA-DC. It generates zones in which the Pd incorporation was definitely greater, apart from particles also being very compacted/densified. These values of H_2-permeance have been increased after a thermal treatment with air while maintaining a complete H_2/N_2 ideal separation factor, apart from mitigating a permanent inhibition of the permeation capacity in the presence of CO.

The versatility of the ELP-PP method to synthesize Pd-based membranes should be highlighted since all membranes demonstrated a very stable behavior with excellent thermal and mechanical resistances throughout the entire set of experiments – independently of the size of CeO_2 particles and the material used for the intermediate layer –, particularly under the IN-OUT configuration mode that makes possible the occurrence of delamination of the Pd external layer.

CRediT authorship contribution statement

M. Salomé Macedo: Investigation, Formal analysis, Writing – original draft. **N. Acha Uriarte:** Investigation, Formal analysis. **M.A. Soria:** Formal analysis, Writing – review & editing. **Luis M. Madeira:** Formal analysis, Writing – review & editing. **J.A. Calles:** Writing – review & editing, Funding acquisition. **R. Sanz:** Writing – review & editing, Supervision. **D. Alique:** Conceptualization, Methodology, Supervision, Formal analysis, Writing – review & editing.

Declaration of Competing Interest

The authors declare that they have no known competing financial interests or personal relationships that could have appeared to influence the work reported in this paper.

Data availability

Data will be made available on request.

Acknowledgments

This work was financially supported by i) Spanish Research Estate Agency through the project of reference PID2020-117273RB-I00, and ii) Base Funding – LA/P/0045/2020 of the Associate Laboratory in Chemical Engineering (ALiCE) and UIDB/00511/2020 – UIDP/00511/2020 of the Laboratory for Process Engineering, Environment, Biotechnology and Energy (LEPABE) – through the national funds provided by FCT/MCTES (PIDDAC).

Moreover, M. Salomé Macedo is especially grateful to the Portuguese Foundation for Science and Technology (FCT) for her Ph.D. grant (SFRH/BD/137106/2018) with national funds of the Ministry of Science, Technology and Higher Education and the European Social Fund (ESF) through the Human Capital Operational Programme (POCH). Finally, M. A. Soria also thanks the FCT for the financial support of his work contract through the Scientific Employment Support Program (Norma Transitória DL 57/2017).

Appendix A. Supplementary data

Supplementary data to this article can be found online at https://doi.org/10.1016/j.seppur.2023.124932.

References

[1] D. Sanz-Villanueva, D. Alique, A.J. Vizcaíno, J.A. Calles, R. Sanz, On the long-term stability of Pd-membranes with TiO_2 intermediate layers for H_2 purification, Int. J. Hydrogen Energy 47 (2022) 11402–11416.
[2] M.S. Macedo, M.A. Soria, L.M. Madeira, Process intensification for hydrogen production through glycerol steam reforming, Renew. Sustain. Energy Rev. 146 (2021), 111151.
[3] S.E. Hosseini, M.A. Wahid, Hydrogen production from renewable and sustainable energy resources: Promising green energy carrier for clean development, Renew. Sustain. Energy Rev. 57 (2016) 850–866.
[4] L. Mosca, J.A. Medrano Jimenez, S.A. Wassie, F. Gallucci, E. Palo, M. Colozzi, S. Taraschi, G. Galdieri, Process design for green hydrogen production, Int. J. Hydrogen Energy 45 (2020) 7266–7277.
[5] S. Shiva Kumar, H. Lim, An overview of water electrolysis technologies for green hydrogen production, Energy Rep. 8 (2022) 13793–13813.
[6] S. Anwar, F. Khan, Y. Zhang, A. Djire, Recent development in electrocatalysts for hydrogen production through water electrolysis, Int. J. Hydrogen Energy 46 (2021) 32284–32317.
[7] X. Li, X. Sun, Q. Song, Z. Yang, H. Wang, Y. Duan, A critical review on integrated system design of solar thermochemical water-splitting cycle for hydrogen production, Int. J. Hydrogen Energy 47 (2022) 33619–33642.
[8] M. Orfila, D. Sanz, M. Linares, R. Molina, R. Sanz, J. Marugán, J.Á. Botas, H_2 production by thermochemical water splitting with reticulated porous structures of ceria-based mixed oxide materials, Int. J. Hydrogen Energy 46 (2021) 17458–17471.
[9] S. Farzad, M.A. Mandegari, J.F. Görgens, A critical review on biomass gasification, co-gasification, and their environmental assessments, Biofuel Res. J. 3 (2016) 483–495.

[10] M.S. Macedo, E. Kraleva, H. Ehrich, M.A. Soria, L.M. Madeira, Hydrogen production from glycerol steam reforming over Co-based catalysts supported on La_2O_3, $AlZnO_x$ and $AlLaO_x$, Int. J. Hydrogen Energy 47 (2022) 33239–33258.
[11] C. Rocha, M.A. Soria, L.M. Madeira, Olive mill wastewater valorization through steam reforming using hybrid multifunctional reactors for high-purity H_2 production, Chem. Eng. J. 430 (2022), 132651.
[12] P.J. Megía, A. Carrero, J.A. Calles, A.J. Vizcaíno, Hydrogen production from steam reforming of acetic acid as a model compound of the aqueous fraction of microalgae HTL using Co-M/SBA-15 (M: Cu, Ag, Ce, Cr) catalysts, Catalysts 9 (2019) 1013.
[13] Y. Shinoda, M. Takeuchi, N. Dezawa, Y. Komo, T. Harada, H. Takasu, Y. Kato, Development of a H_2-permeable $Pd_{60}Cu_{40}$-based composite membrane using a reverse build-up method, Int. J. Hydrogen Energy 46 (2021) 36291–36300.
[14] Y.-J. Wu, P. Li, J.-G. Yu, A.F. Cunha, A.E. Rodrigues, High-purity hydrogen production by sorption-enhanced steam reforming of ethanol: A cyclic operation simulation study, Ind. Eng. Chem. Res. 53 (2014) 8515–8527.
[15] G. Bernardo, T. Araújo, T. da Silva Lopes, J. Sousa, A. Mendes, Recent advances in membrane technologies for hydrogen purification, Int. J. Hydrogen Energy 45 (2020) 7313–7338.
[16] M. Yáñez, F. Relvas, A. Ortiz, D. Gorri, A. Mendes, I. Ortiz, PSA purification of waste hydrogen from ammonia plants to fuel cell grade, Sep. Purif. Technol. 240 (2020), 116334.
[17] N.A. Al-Mufachi, N.V. Rees, R. Steinberger-Wilkens, Hydrogen selective membranes: A review of palladium-based dense metal membranes, Renew. Sustain. Energy Rev. 47 (2015) 540–551.
[18] A.E. Rodrigues, L.M. Madeira, Y.-J.-A. Wu, R.A. Faria, Sorption enhanced reaction processes, World Scientific, 2017.
[19] F. Gallucci, E. Fernandez, P. Corengia, M. van Sint Annaland, Recent advances on membranes and membrane reactors for hydrogen production, Chem. Eng. Sci. 92 (2013) 40–66.
[20] T. Peters, A. Caravella, Pd-based membranes: overview and perspectives, Membranes 9 (2019) 25.
[21] D. Martinez-Diaz, D. Martínez del Monte, E. García-Rojas, D. Alique, J.A. Calles, R. Sanz, Comprehensive permeation analysis and mechanical resistance of electroless pore-plated Pd-membranes with ordered mesoporous ceria as intermediate layer, Sep. Purif. Technol. 258 (2021), 118066.
[22] J. Melendez, E. Fernandez, F. Gallucci, M. van Sint Annaland, P.L. Arias, D. A. Pacheco Tanaka, Preparation and characterization of ceramic supported ultra-thin (~1μm) Pd-Ag membranes, J. Membr. Sci. 528 (2017) 12–23.
[23] M. Dehghani Mobarake, P. Jafari, M. Irani, Preparation of Pd-based membranes on Pd/TiO_2 modified NaX/PSS substrate for hydrogen separation: Design and optimization, Microporous Mesoporous Mater. 226 (2016) 369–377.
[24] A. Bottino, M. Broglia, G. Capannelli, A. Comite, P. Pinacci, M. Scrignari, F. Azzurri, Sol–gel synthesis of thin alumina layers on porous stainless steel supports for high temperature palladium membranes, Int. J. Hydrogen Energy 39 (2014) 4717–4724.
[25] T. Van Gestel, F. Hauler, M. Bram, W.A. Meulenberg, H.P. Buchkremer, Synthesis and characterization of hydrogen-selective sol–gel SiO_2 membranes supported on ceramic and stainless steel supports, Sep. Purif. Technol. 121 (2014) 20–29.
[26] I. Contardi, L. Cornaglia, A.M. Tarditi, Effect of the porous stainless steel substrate shape on the ZrO_2 deposition by vacuum assisted dip-coating, Int. J. Hydrogen Energy 42 (2017) 7986–7996.
[27] E. Fernandez, J.A. Medrano, J. Melendez, M. Parco, J.L. Viviente, M. van Sint Annaland, F. Gallucci, D.A. Pacheco Tanaka, Preparation and characterization of metallic supported thin Pd–Ag membranes for hydrogen separation, Chem. Eng. J. 305 (2016) 182–190.
[28] L. Furones, D. Alique, Interlayer properties of in-situ oxidized porous stainless steel for preparation of composite Pd membranes, ChemEngineering (2018).
[29] Y. Yan, R. Bateni, J. Harris, O. Kesler, Fabrication of reactive element oxide coatings on porous ferritic stainless steel for use in metal-supported solid oxide fuel cells, Surf. Coat. Technol. 272 (2015) 415–427.
[30] D. Martinez-Diaz, V. Michienzi, J.A. Calles, R. Sanz, A. Caravella, D. Alique, Versatile and resistant electroless pore-plated Pd-membranes for H_2-separation: Morphology and performance of internal layers in PSS tubes, Membranes (Basel) 12 (2022).
[31] D. Alique, D. Martinez-Diaz, R. Sanz, J.A. Calles, Review of supported Pd-based membranes preparation by electroless plating for ultra-pure hydrogen production, Membranes 8 (2018) 5.
[32] J. Tong, Y. Matsumura, H. Suda, K. Haraya, Thin and dense Pd/CeO_2/MPSS composite membrane for hydrogen separation and steam reforming of methane, Sep. Purif. Technol. 46 (2005) 1–10.
[33] R. Sanz, J.A. Calles, D. Alique, L. Furones, New synthesis method of Pd membranes over tubular PSS supports via “pore-plating” for hydrogen separation processes, Int. J. Hydrogen Energy 37 (2012) 18476–18485.
[34] D. Martinez-Diaz, D. Alique, J.A. Calles, R. Sanz, Pd-thickness reduction in electroless pore-plated membranes by using doped-ceria as interlayer, Int. J. Hydrogen Energy 45 (2020) 7278–7289.
[35] D. Martinez-Diaz, R. Sanz, J.A. Calles, D. Alique, H_2 permeation increase of electroless pore-plated Pd/PSS membranes with CeO_2 intermediate barriers, Sep. Purif. Technol. 216 (2019) 16–24.
[36] A. Arratibel, J.A. Medrano, J. Melendez, D.A. Pacheco Tanaka, M. van Sint Annaland, F. Gallucci, Attrition-resistant membranes for fluidized-bed membrane reactors: Double-skin membranes, J. Membr. Sci. 563 (2018) 419–426.
[37] J.-Y. Han, C.-H. Kim, H. Lim, K.-Y. Lee, S.-K. Ryi, Diffusion barrier coating using a newly developed blowing coating method for a thermally stable Pd membrane deposited on porous stainless-steel support, Int. J. Hydrogen Energy 42 (2017) 12310–12319.
[38] D. Alique, M. Imperatore, R. Sanz, J.A. Calles, M. Giacinti Baschetti, Hydrogen permeation in composite Pd-membranes prepared by conventional electroless plating and electroless pore-plating alternatives over ceramic and metallic supports, Int. J. Hydrogen Energy 41 (2016) 19430–19438.
[39] A.L. Mejdell, D. Chen, T.A. Peters, R. Bredesen, H.J. Venvik, The effect of heat treatment in air on CO inhibition of a ~3μm Pd–Ag (23wt.%) membrane, J. Membr. Sci. 350 (2010) 371–377.
[40] A. Ramachandran, W.M. Tucho, A.L. Mejdell, M. Stange, H.J. Venvik, J. C. Walmsley, R. Holmestad, R. Bredesen, A. Borg, Surface characterization of Pd/Ag23wt% membranes after different thermal treatments, Appl. Surf. Sci. 256 (2010) 6121–6132.
[41] A.D. Kiadehi, M. Taghizadeh, Fabrication, characterization, and application of palladium composite membrane on porous stainless steel substrate with NaY zeolite as an intermediate layer for hydrogen purification, Int. J. Hydrogen Energy 44 (2019) 2889–2904.
[42] C.V. Miguel, A. Mendes, S. Tosti, L.M. Madeira, Effect of CO and CO_2 on H_2 permeation through finger-like Pd–Ag membranes, Int. J. Hydrogen Energy 37 (2012) 12680–12687.
[43] M.A. Soria, C. Rocha, S. Tosti, A. Mendes, L.M. Madeira, CO_x free hydrogen production through water-gas shift reaction in different hybrid multifunctional reactors, Chem. Eng. J. 356 (2019) 727–736.
[44] S. Tosti, C. Cavezza, M. Fabbricino, L. Pontoni, V. Palma, C. Ruocco, Production of hydrogen in a Pd-membrane reactor via catalytic reforming of olive mill wastewater, Chem. Eng. J. 275 (2015) 366–373.
[45] N.S. Patki, S.-T.-B. Lundin, J.D. Way, Apparent activation energy for hydrogen permeation and its relation to the composition of homogeneous PdAu alloy thin-film membranes, Sep. Purif. Technol. 191 (2018) 370–374.
[46] W.-H. Chen, S.-W. Lin, C.-Y. Chen, Y.-H. Chi, Y.-L. Lin, Impact of vacuum operation on hydrogen permeation through a palladium membrane tube, Int. J. Hydrogen Energy 44 (2019) 14434–14444.
[47] M. Sarić, Y.C. van Delft, R. Sumbharaju, D.F. Meyer, A. de Groot, Steam reforming of methane in a bench-scale membrane reactor at realistic working conditions, Catal. Today 193 (2012) 74–80.
[48] Y. Huang, R. Dittmeyer, Preparation of thin palladium membranes on a porous support with rough surface, J. Membr. Sci. 302 (2007) 160–170.
[49] D. Sanz-Villanueva, D. Alique, A.J. Vizcaíno, R. Sanz, J.A. Calles, Pre-activation of SBA-15 intermediate barriers with Pd nuclei to increase thermal and mechanical resistances of pore-plated Pd-membranes, Int. J. Hydrogen Energy 46 (2021) 20198–20212.